Physics – Uspekhi **45** (10) 1001 – 1018 (2002)

REVIEWS OF TOPICAL PROBLEMS

PACS numbers: 52.40.Mj, 52.75.Pv, 52.80.Mg, 52.80.Vp

Mechanism of anomalous ion generation in vacuum arcs

G A Mesyats, S A Barengol'ts

DOI: 10.1070/PU2002v045n10ABEH001247

Contents

Abstract. A model for the generation of an ion flow in a vacuum arc is proposed, based upon the analysis of ecton processes. It is shown that the charge states and the velocities of directed motion of the ions result from cathode microsections being explosively destroyed by Joule heating with a high-density current. In this case, the ionization processes occur within a narrow (of the order of a micrometer) region near the cathode, and thereafter the ionic composition of the plasma remains unchanged. For arc currents of up to a kiloampere, a current increase simply increases the number of simultaneously operating ectons, thus explaining the weak experimental dependence of ion flow parameters on the vacuum arc current.

1. Introduction

Amongst the most interesting physical effects accompanying the operation of a vacuum arc discharge are the appearance of anomalous ions in the discharge plasma. The ion anomaly is associated with the fact that they move primarily in the direction opposite to that obeying the laws of electricity — from the cathode to the anode. The energies of these ions far exceed the energy corresponding to the voltage applied to the interelectrode gap. Typical values of the voltage drop across an arc discharge in the subkiloampere current range lie between 10 – 30 V, whilst the ion energies are at a level of 30 – 150 eV [1 – 3]. Furthermore, multiply charged positive ions were quite unexpectedly found to present in vacuum arc plasmas [2 – 4], the ions with charges of higher than +2 constituting the absolute majority for some cathode materials (W, Mo, Cr, etc.).

Since the discovery of anomalous ion properties, discussions are underway concerning the physical processes responsible for their emergence. A paradoxical situation has ensued: the ions of a vacuum arc plasma have found wide technological use, including ion-plasma spraying, coating, ion implantation, etc. [4], and yet there is no consensus of opinion regarding the mechanism of their production.

Remarkable progress in the study of the vacuum discharge was achieved owing to the discovery of explosive electron emission in 1966 [5]. The current of a vacuum spark was established to be the current of emission emerging as a result of microscopic explosions on the cathode surface. A detailed investigation of the phenomenon of explosive electron emission showed [6 – 8] that the operation of the cathode spots in a vacuum spark and a vacuum arc is controlled by common physical processes. Ectons — separate portions of electrons emitted during explosive electron emission — underlie these processes [3].

Our review is a logical continuation of the investigations [5 – 8] pursued at the Institute of High-Current Electronics, Siberian Branch of the Russian Academy of Sciences (Tomsk) and the Institute of Electrophysics, Ural Branch of the Russian Academy of Sciences (Ekaterinburg) in the field of a vacuum discharge. The results of studies of the physical processes leading to the vacuum breakdown, a description of the phenomenon of explosive electron emission [6, 7], and a hypothesis for the ectonic operation mechanism of the cathode spot in a vacuum spark and an arc [8] were presented in earlier reviews.

The decisive role of explosive emission processes in the operation of a vacuum arc discharge has long been questioned, but recently obtained data unambiguously count in their favor. Theoretically, this is primarily the construction of an ectonic model of the cathode spot in a vacuum discharge [3] whereby it was possible to describe from a unified standpoint the processes following in spark and arc vacuum discharges.

The main concepts of the ectonic model were additionally confirmed by the measurement data on the energy of ion

G A Mesyats Institute of Electrophysics, Ural Branch of the Russian Academy of Sciences,
ul. Amundsena 106, 620016 Ekaterinburg, Russian Federation
Tel. (7-095) 237 53 12. Fax (7-095) 952 50 81
E-mail: mesyats@pran.ru
S A Barengol'ts Institute of Electrophysics, Ural Branch of the Russian Academy of Sciences,
ul. Amundsena 106, 620016 Ekaterinburg, Russian Federation
Tel./Fax (7-095) 234 31 63
E-mail: sb@nsc.gpi.ru

Received 20 May 2002, revised 5 June 2002
Uspekhi Fizicheskikh Nauk **172** (10) 1113 – 1130 (2002)
Translated by E N Ragozin; edited by A Radzig

directed motion in an arc plasma under high vacuum [9], and also by the investigations of the cathode spot structure in a vacuum arc, performed with a high spatial and time resolution [10]. The gas dynamic mechanism of ion acceleration in an arc discharge and the evidence for the existence of cathode spot cells with tens of nanoseconds long lifetimes, found in these works, have made it possible to eliminate the main arguments adduced against the explosive emission nature of the phenomena in a vacuum arc.

The existence of a common mechanism for the cathode processes in vacuum arcs and sparks allowed the researchers to combine the results of seemingly independent investigations into different stages of the vacuum discharge and to obtain a clear picture of the physical effects responsible for the production of ions in a vacuum arc.

The opening sections of our review present experimental data on the measurements of the main parameters of the ion stream (energies of directed motion, charge-state distributions, and ion erosion) in vacuum arcs. Given next are an analysis of the contemporary investigations of the cathode processes in a vacuum arc, the formulation of the basic concepts concerning the ectonic model of a cathode spot, the estimates of ion parameters in the framework of this model, and the results of numerical simulations of ectonic processes.

2. Ion flow parameters in vacuum arcs

2.1 Ion energies

2.1.1 Average ion velocities. Tanberg [11] was the first to discover high-velocity particle flows emanating from the cathode spot region of a vacuum arc. The reactive force of this flux proved to be proportional to the arc current with a coefficient of 20 dyn A^{-1} for a copper cathode. The same force acted on an electrode suspended in front of the cathode, repelling it from the cathode. By measuring the recoil momentum, Tanberg determined the particle velocity which was equal to 1.6×10^6 cm s^{-1}. If it is assumed that the plasma jet is purely thermal in nature, the vapor temperature in the vicinity of the cathode spot should be of the order of 5×10^5 K. Tanberg observed that the spectroscopic measurements of exploding-wire plasma radiation yielded a temperature falling within this region.

At about the same time, Kobel [12] made an independent estimate of the velocity of an outward jet from a mercury cathode spot to obtain a value in the $(1.6-4.3) \times 10^6$ cm s^{-1} range. These jets were long believed to consist of neutral atomic particles, since nobody could assume that plasma jets comprising positive ions could move in the 'opposite' direction — from the cathode to the anode.

Subsequent investigations in this area were performed by Plyutto's group [13]. In the experiments [13], the discharge chamber was equipped with a pendular meter of the jet momentum, an electrostatic analyzer, and a Thompson mass spectrometer. This allowed them to obtain comprehensive data on the charge composition and the average velocity of cathode jets, and on the ion energy distribution for a number of metallic cathodes.

For metals with a relatively high boiling temperature, like Cu, Ag, and Mg, the degree of ionization of the cathode plasma was 50 – 100%, with doubly and triply charged ions also being observed in it, and the velocity of plasma jets was of the order of 10^6 cm s^{-1}. For readily evaporable Zn and Cd, the plasma jet velocity proved to be somewhat lower, and the degree of ionization of metal vapor was in the 10 – 25% range. The ion energies ranged from 0 to 70 eV. The occurrence of such a high energy permitted ions to move not only towards the cathode, as was previously assumed, but in the opposite direction as well.

The presence of high-energy ions in the plasma jets led Plyutto et al. [13] to conclude that there exists an electric potential hump in the plasma cathode spot region. Despite the fact that the results of paper [13] were later improved and supplemented, while the inference regarding the existence of the potential hump was not borne out, we can state that it has been this work which has served as a basis for harnessing the vacuum arc ions in implantation technologies.

Practically simultaneously with work [13], Mesyats and his associates showed that similar plasma jets are present at the spark stage of a vacuum discharge [14 – 16]. For instance, their velocity was equal to 2×10^6 cm s^{-1} for a copper cathode and was caused by microexplosions on the cathode surface, which were attended by explosive electron emission [15]. Mesyats [16] showed that this value of the plasma jet velocity can be obtained if it is assumed that there occurs an explosive gas dynamic expansion of the cathode plasma, when specific energies corresponding to the electric explosion of the metal are added to the cathode material.

2.1.2 Charge state effect. Davis and Miller [17] made an attempt to refine the data of work [13]. They investigated the ionic composition and the arc-plasma ion energy distribution for nine different cathode materials. The ion energy spectrum was made up of broad lines which were almost symmetric about their peaks. The spectrum can be characterized by three parameters: the peak intensity, the energy corresponding to the peak intensity (the most probable or average energy), and the full width at half peak intensity of the line.

The simultaneous consideration of peak energies and ion line widths revealed that a great quantity of ions possess energies which correspond to a higher potential than the voltage drop across the arc. For a wide variety of materials, the average ion energy also proved to be higher than the energy corresponding to the potential difference applied to the interelectrode gap. As for a vacuum spark, the average ion velocities were found to be about 10^6 cm s^{-1}.

In Fig. 1 we show the ratios between the most probable ion energy and the ion charge (in units of electron charge) as functions of the arc current, which were measured for singly, doubly, and triply ionized atoms of the cathode material. The voltage whereby a given ion acquires energy equal to the most probable value is plotted on the ordinate axis. The arc current is plotted on the logarithmic abscissa. The data were obtained in the current range up to 300 A, where the cathode is the only source of metal vapor.

Some misunderstandings arose in the interpretation of the measurement data given in Fig. 1. The issue is that the ion kinetic energy was in many papers estimated as $W = eQU$, where Q is the ion charge. The thus obtained energies of singly, doubly, and triply ionized Cu atoms are equal to 57, 96, and 126 eV, respectively, for an arc current of 100 A. However, as noted in Ref. [18], one should subtract the plasma potential approximately equal to the voltage drop across the arc from the potential corresponding to the peak of the ion distribution function. In this case, the difference in the ion energy would no longer be that significant. In particular,

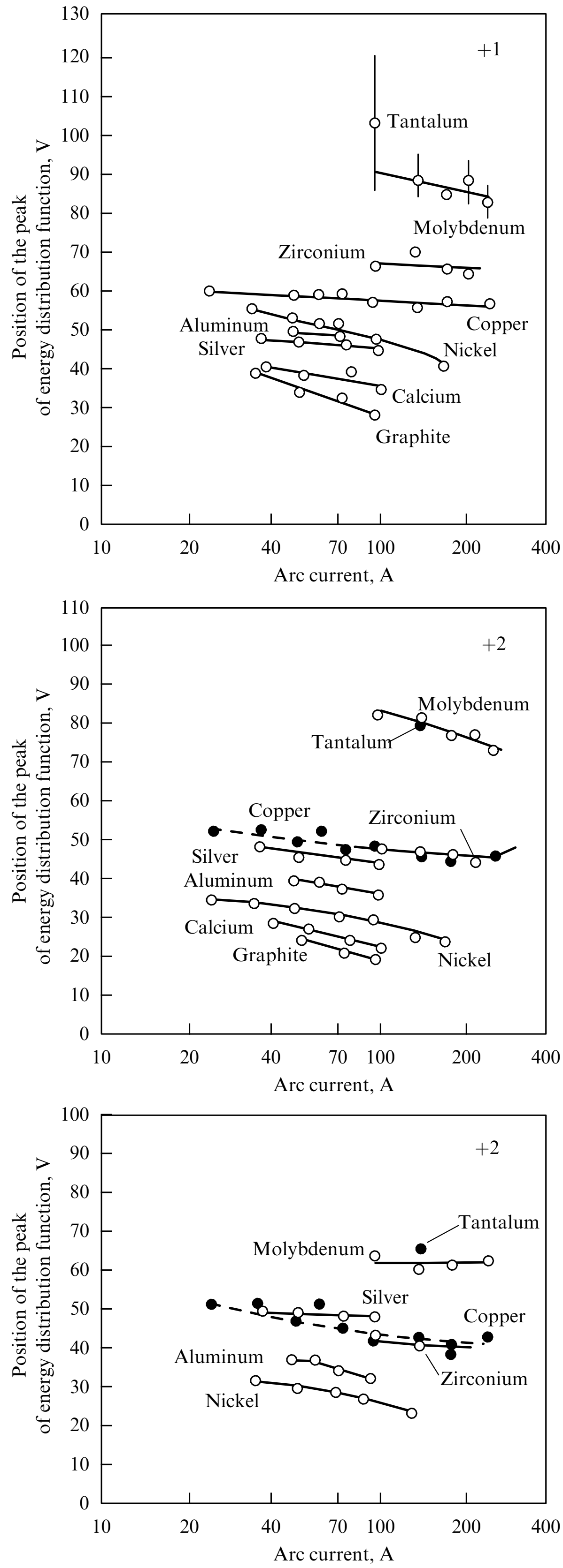

Figure 1. Most probable energy values of singly, doubly, and triply ionized atoms emitted by vacuum arcs with the cathodes made from different materials as functions of the arc current. The potential of the ion collector is equal to that of the cathode [17].

the respective energies of singly, doubly, and triply ionized atoms would be equal to 37, 56, and 66 eV.

According to the assumption that there exists a potential hump, the ion energy should be directly proportional to the ion multiplicity. On the other hand, in the case of monotonic potential growth and, hence, the gas dynamic acceleration mechanism, the energies of ions of different multiplicities should be equal. The results obtained in Ref. [17] were indicative of some dependence of the ion energies on the ion multiplicity. However, this dependence turned out to be much weaker than one would expect on the basis of the potential hump model.

The measurement data on ion velocities at different distances (20 – 140 mm) in the direction perpendicular to the axis of the electrodes also proved to be ambiguous [19].The velocities of fastest Cu and Ag ions were equal to 2.1×10^6 and 1.6×10^6 cm s^{-1}, respectively, and were independent of the ion multiplicity. However, these ions were produced at the initial point in time (for about 3 μs). At a later stage (after 10 μs), the ion energy was observed to depend slightly on the ion multiplicity. The respective velocities of singly, doubly, and triply charged ions were found to equal 1.3×10^6, 1.4×10^6, and 1.7×10^6 cm s^{-1} for copper cathodes, and 0.8×10^6, 1.1×10^6, and 1.4×10^6 cm s^{-1} for silver cathodes.

The uncertainty regarding the acceleration mechanism of the plasma ions in a vacuum arc persisted until the emergence of the paper by Oks and his co-workers [20]. In their experiments, the ions extracted from the plasma were accelerated by a dc voltage of 10 – 25 kV in a multiaperture three-grid system. The charge distribution of the accelerated ion flow was analyzed employing a time-of-flight spectrometer. The ion velocities were measured from the delay time between the weak arc-current perturbation and the response of the ion current extracted.

An analysis of the evolution of currents caused by different-multiplicity ions allowed the measurement of their velocities of directed motion. The perturbation was produced by either a short-duration jump of the arc current, or by its forced termination. As revealed by the experiments, the temporal responses of differently charged ions to the jump or termination of the arc current were largely similar for each cathode material, which signified that the kinetic energies of ions of different multiplicities were equal (Fig. 2)

The authors of Ref. [20] revealed why their findings were different from the ion energies measured by Davis and Miller [17]. The point is that the pumping techniques employed in the experiments of Ref. [17] could not afford a high vacuum owing to a strong gas release during the arc burning. To verify the effect of residual gas pressure, the experiments were staged to measure the velocities of directed ion motion under the conditions of forced gas puffing into the discharge gap.

Experiments of Ref. [20] revealed that the impairment of vacuum conditions resulted in different decreases in the velocities characterizing directed motion of ions of various multiplicity. For relatively high residual gas pressures ($p > 10^{-2}$ Pa), the values of ion velocity proved to be close to those measured in Ref. [17]. This fact is indirectly confirmed by the data of Yang et al. [21] who showed that increasing the pressure from 0.01 to 1 Pa resulted in a reduction of the highest energy of titanium ions from 75 to 55 eV, and a reduction of the average ion energy from 35 to 10 eV.

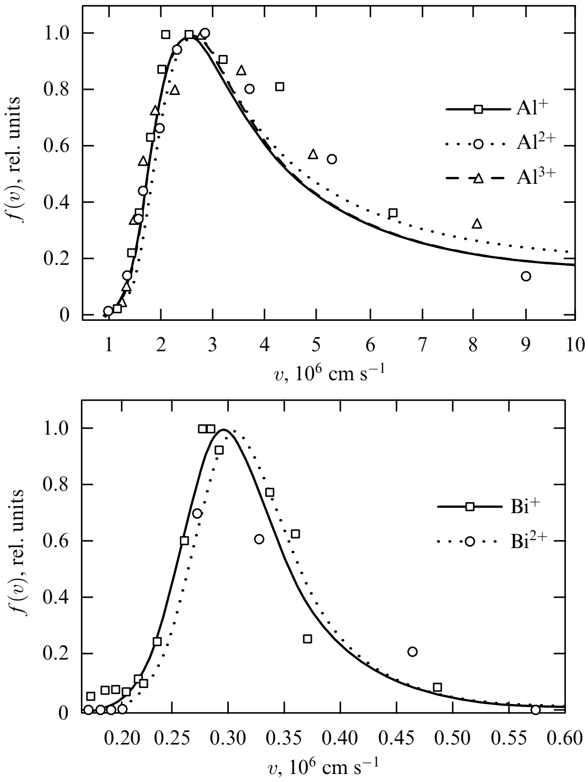

Figure 2. Ion velocity distribution functions for vacuum arcs with aluminum and bismuth cathodes [20].

It is pertinent to note that despite the established fact of equality between the velocities of ions of different multiplicity there exists a significant scatter (up to 35%) in the absolute values of measured ion velocities, depending on the measuring technique (a jump or termination of the arc current). Yushkov et al. [9] took advantage of a modified technique whereby an *LC* circuit was introduced into the electric circuit to allow the modulation of the arc current. The average velocity and ion energy data measured by this technique are collected in Table 1.

Although the findings of Ref. [9] necessitate refinement, it may be deduced that ion velocities are of the order of 10^6 cm s^{-1} for virtually all conducting materials. Similar ion velocities were also derived by different methods in studies of a spark discharge in vacuum [22], when the initial stages of origination of a cathode spot for $10^{-9}-10^{-6}$ s were of interest. This is indicative of a common ion acceleration mechanism in vacuum arcs and sparks.

Table 1. Average velocity and kinetic energy of the arc plasma ions for different cathode materials [9].

Cathode material	Atomic number	Ion velocity, 10^4 m s^{-1}	Kinetic energy, eV
Li	3	2.38	20
C	6	2.97	54
Mg	12	3.06	117
Al	13	2.76	106
Si	14	2.58	97
Ca	20	2.59	140
Ti	22	2.22	122
V	23	1.93	97
Cr	24	1.94	101
Mn	25	1.08	33
Fe	26	1.18	40
Co	27	1.18	43
Ni	28	1.09	36
Cu	29	1.28	54
Zn	30	1.04	36
Ge	32	1.10	45
Y	39	1.43	94
Zr	40	1.57	116
Nb	41	1.55	116
Mo	42	1.74	151
Rh	45	1.57	131
Ag	47	1.04	61
Cd	48	0.68	27
In	49	0.55	18
Sn	50	0.75	34
Sb	51	0.52	17
Ba	56	0.67	32
La	57	0.70	35
Ce	58	0.70	36
Pr	59	0.87	55
Sm	62	0.74	43
Eu	63	0.78	48
Gd	64	0.74	45
Tb	65	0.74	45
Dy	66	0.74	46
Ho	67	0.83	58
Er	68	0.82	59
Tm	69	0.83	61
Hf	72	0.92	79
Ta	73	1.14	121
W	74	1.05	106
Pt	78	0.68	47
Au	79	0.58	34
Pb	82	0.54	31
Bi	83	0.42	19
Th	90	0.99	118
U	92	1.14	160

Note. The arc current is $i = 100-200$ A. The data are valid for the points in time $t > 100$ μs after the arc cycle onset.

2.2 Ionic composition

2.2.1 Ion charge-state distribution. In Refs [13, 17] cited above, the presence of multiply charged ions in arc plasmas was experimentally established and the ion charge-state distribution was derived. The investigations into the ionic composition of arc plasmas were given fresh impetus in connection with the development of vacuum arc-based ion sources by Brown's group [23–25].

The distribution of charges drawn out of a plasma holds much significance because it determines the energy of the ion beam being extracted. Increasing the average ion charge permits one to raise the ion beam energy for a constant accelerating voltage, while the high emission capacity of the cathode spot in a vacuum arc makes it possible to obtain intense beams of ions of specific multiplicity even when their fraction in the plasma is relatively small.

Brown [23] presented the results of a charge-state spectrum investigation of the ion beam produced by the 'MEEVA' vacuum-arc ion source. With the aid of the sources of this type, the charge-state distributions of arc-produced ions were derived for practically all conducting materials. The data obtained in these investigations are collected in Table 2 for an arc current of 200 A. It is noteworthy that varying the arc current within the 50–500-A range exerted only a small effect on the ion charge distribution [23–25]. A Faraday cup was employed to measure the ion current. In this case, account was taken of the fact that the electric current $I_e = QI_p$ is Q times higher than the particle flux.

Table 2. Charge-state distribution and average ion charge of an arc plasma for different cathode materials [23].

Cathode material	f_1	f_2	f_3	f_4	f_5	f_6	Z
Li	100						1.00
C	100						1.00
Mg	46	54					1.54
Al	38	51	11				1.73
Si	63	35	2				1.39
Ca	8	91	1				1.93
Sc	27	67	6				1.79
Ti	11	75	14				2.03
V	8	71	20	1			2.14
Cr	10	68	21	1			2.09
Mn	49	50	1				1.53
Fe	25	68	7				1.82
Co	34	59	7				1.73
Ni	30	64	6				1.76
Cu	16	63	20	1			2.06
Zn	80	20					1.20
Ge	60	40					1.40
Sr	2	98					1.98
Y	5	62	33				2.28
Zr	1	47	45	7			2.58
Nb	1	24	51	22	2		3.00
Mo	2	21	49	25	3		3.06
Pd	23	67	9	1			1.88
Ag	13	61	25	1			2.14
Cd	68	32					1.32
In	66	34					1.34
Sn	47	53					1.53
Sb	100						1.00
Ba	0	100					2.00
La	1	76	23				2.22
Ce	3	83	14				2.11
Pr	3	69	28				2.25
Nd	0	83	17				2.17
Sm	2	83	15				2.13
Gd	2	76	22				2.20
Dy	2	66	32				2.30
Ho	2	66	32				2.30
Er	1	63	35	1			2.36
Tm	13	78	9				1.96
Yb	3	88	8				2.03
Hf	3	24	51	21	1		2.89
Ta	2	33	38	24	3		2.93
W	2	23	43	26	5	1	3.07
Ir	5	37	46	11	1		2.66
Pt	12	69	18	1			2.08
Au	14	75	11				1.97
Pb	36	64					1.64
Bi	83	17					1.17
Th	0	24	64	12			2.88
U	0	12	58	30			3.18

Note. The fractions f_i of ions with a charge i are expressed on a percentage basis.

Table 2 also collates the average charge-state values

$$Z = \frac{\sum(fQ)}{\sum f}\,, \tag{1}$$

where f is the fraction of ions in a given charge state. One can see from the data given in Table 2 that the average charge of arc plasma-produced ions lies in the range between $+1$ and $+3$, depending on the cathode material, while in the plasma there are ions with the charges from $+1$ to $+6$. Materials with a lower boiling temperature T_b exhibit, as a rule, a lower average ion charge.

Brown [23] established an empirical relationship between the average particle charge and the boiling temperature:

$$Z = 1 + 0.38\,\frac{T_b}{1000}\,, \tag{2}$$

where T_b is the boiling temperature (in Celsius degrees) of the cathode material. Relationship (2) is in reasonably good accord with the average ion charge data for the materials investigated, with the exception of carbon. Therefore, the investigations revealed that the average ion charge is independent of the conditions of arcing and is only determined by the characteristics of the cathode material.

Relying on the experimental data of Brown's review [23], Anders [26] constructed a periodic table of ion charge distribution in arc plasmas for all metals, carbon, and Si and Ge semiconductors. Apart from the charge distribution, the table lists the values of average ion charge, the neutral particle fraction, and also the effective plasma temperature in the cathode spot and the plasma density for the above-cited elements.

The plasma parameters were derived assuming the existence of local thermodynamic equilibrium in the cathode spot region and the applicability of Saha equations for a weakly nonideal plasma (the Debye – Hückel approximation). Advantage was taken of the fact that the ionic composition 'freezes' during the plasma expansion and its transition to the nonequilibrium state [27]. In this case, the density and temperature fluctuations in the course of 'freezing' were assumed to be small.

As shown by the calculations, the proposed model provides a fairly good description of the available experimental data. In this case, the calculated ion number densities lie mostly in the $10^{17} - 10^{19}$-cm^{-3} range, and the plasma temperature lies between 1.5 and 4.5 eV. Anders [26] recognized two problematic groups of elements. In the first group, which is dominated by only singly or doubly charged ions (Li, C, Zn, Sr, Cd, Sn, Sb, Ba, and Pb), there exists a large uncertainty in the plasma temperature (± 0.5 eV) and the plasma density in the freezing of the charge-state composition (plus-minus an order of magnitude or even more). The second group comprises materials (Mo, Ag, Hf, Ta, W, and Ir) for which the charge-state distribution established experimentally is significantly broader than the calculated one. This was attributed to the transient character of the processes in the cathode spot of a vacuum arc.

Indeed, the experiments showed that increasing the duration of an arc current pulse from 3 to 600 μs results in a reduction of the average ion charge by 10 – 30% [28]. However, in our view this is related to the features of the discharge spark-to-arc stage transformation. The transient process is accompanied by a significantly higher (by almost a factor of two – three) energy release in comparison with the arc discharge [28], resulting in a growth of the electron temperature in the cathode region and the consequential increase in the average ion charge.

The cause of disagreement with the experimental data lies with the fact that the dense near-cathode plasma production mechanism itself was not determined in Ref. [26]. Barengol'ts et al. [29] showed that the plasma ionic composition is largely determined by the ion velocity build-up rate, and therefore the plasma parameters (temperature, density) derived by the author of paper [26] through the calculations cannot unambiguously represent the actual plasma parameters in the spot region.

It is noteworthy that there exists some scatter in the experimental results obtained at the facility employed in Ref. [23] or at the analogous ones. In particular, the average ion charge measured in Refs [24, 25] turned out to be lower by 10 – 15%. Conceivably the distinction between the data might stem from the difference in vacuum conditions in the pursuance of the research. Nikolaev et al. [30] showed that increasing the residual gas pressure lowers the fraction of multiply charged ions in a plasma.

The data collected in Table 2 are close to the plasma ionic composition at the initial stage of cathode flare expansion in the spark stage of a vacuum discharge [22]. In particular, spectrometric investigations for an aluminum cathode revealed the presence of ions with charges from +1 to +3, with doubly charged aluminum ions comprising the majority of ions.

2.2.2 Effect of an axial magnetic field. In conclusion we discuss the interesting results obtained in investigating the effect of a longitudinal magnetic field and an arc current on the ion charge-state distribution [31 – 33]. These investigations showed that producing a strong magnetic field in the arc discharge plasma results in a drastic reduction of the singly and doubly charged ion fractions with a simultaneous augmentation of the multiply charged component.

The fractions of different-multiplicity ions measured for an arc in the magnetic field are collected in Table 3. A similar effect was observed when the arc current exceeded a value of 1 kA. In this case, the intrinsic magnetic field of the arc was equal to about 1 kG and was comparable to the external magnetic field which exerted an observable effect on the ionic composition. It is vital to note that appreciable fractions of the previously unobserved components in the charge-state spectrum of discharge ions (C^{3+}, Ti^{5+}, Cr^{5+}, Ni^{5+}, Ni^{6+}, etc.) manifested themselves in the presence of a strong magnetic field.

Table 3. Charge-state distribution and the average charge Z_f of an arc plasma embedded in an external axial magnetic field [31].

Cathode material	Z	f_1	f_2	f_3	f_4	f_5	f_6	Z_f	Z_f/Z
C	1.0	60	40					1.4	1.40
Mg	1.5	5	95					1.9	1.27
Al	1.7	10	40	50				2.4	1.40
Sc	1.9	16	23	59	2			2.5	1.31
Ti	2.0	5	35	54	6			2.6	1.30
V	2.1	13	31	48	8			2.5	1.20
Cr	2.0	11	26	55	8			2.6	1.30
Mn	1.5	26	47	25	2			2.0	1.33
Fe	1.8	7	58	35				2.3	1.28
Ni	1.6	19	62	18	1			2.0	1.25
Co	1.8	9	56	31	4			2.3	1.27
Cu	1.9	8	41	47	3	1		2.5	1.32
Y	2.2	6	9	77	8			2.9	1.32
Nb	2.7	1	9	23	52	13	2	3.7	1.37
Mo	2.8	5	11	26	48	10		3.5	1.25
Ba	2.0	2	41	53	3	1		2.6	1.30
La	2.3	3	16	61	20			3.0	1.30
Gd	2.0	1	43	41	15			2.7	1.35
Er	2.2	2	12	70	16			3.0	1.36
Hf	2.8	5	16	31	32	15	1	3.4	1.21
Ta	3.3	1	5	13	40	41	2	4.2	1.27
W	3.4	1	5	16	39	32	7	4.2	1.20
Pt	2.1	3	25	64	8			2.8	1.30
Pb	1.6	1	75	24				2.2	1.37
Bi	1.1	9	60	31				2.2	2.00

Note. The arc current is $i = 220$ A, and the magnetic field $B = 3.75$ kG. The fractions f_i of ions with a charge i are expressed on a percentage basis.

A strict correlation was experimentally established between the increase in average ion charge and the rise in operating arc voltage. For instance, for the strongest magnetic field and arc current, which afforded the largest fraction of highly charged ions, the voltage drop across the arc amounted to 100 – 120 V and was five – six times higher than the initial voltage level.

2.3 Ion erosion

2.3.1 Ion current toward the anode. Investigations into the energy distribution of arc plasma ions revealed that they escape from the cathode spot region with the velocities to an order of 10^6 cm s^{-1}. These ions produce a current opposed to the arc current, for their motion is directed primarily from the cathode to the anode. Using cylindrical screens, Kimblin [34, 35] measured the ion currents emerged from the cathode spots of a vacuum arc as functions of the arc current, the electrode material and size, the interelectrode distance, the screen diameter, and the voltage applied to the screen.

The investigations [34, 35] revealed that the ion current collected on the cylindrical screen attained a limiting value which was independent of the geometric parameters, was approximately proportional to the total arc current, and depended only slightly on the cathode material. Kimblin interpreted this limiting current as the total ion current delivered by the cathode spots into the arc gap. For currents lower than 10^3 A, it was recognized that the proportionality coefficient between the ion current i_i and the total current is 0.07 – 0.1 for 16 cathode materials under investigation (Cd, Zn, Ca, Pb, Mg, Au, Ga, Cu, Sn, Cr, Fe, Ti, C, Mo, Ta, and W).

We emphasize that the current in the anode circuit was purely electron current, because all the ions were extracted from the arc gap. Since the 16 materials specified above embrace a very broad range of material properties, it is believed that the ion-to-electron current ratio is the most important parameter which characterizes the operation of a cathode spot. The angular distribution of the ion flux peaks in the direction perpendicular to the cathode surface [13, 36].

2.3.2 Cathode erosion products. The ion current from a cathode has the effect that the cathode loses its mass in the form of escaping ions. It is precisely the production of a conducting medium in the interelectrode gap that determines the operation of a vacuum discharge. The measure of ion erosion is the erosion rate γ_i, i.e. the ratio between the mass carried away in the form of ions and the charge flowed $q = i\,\Delta t$, where i is the arc current. The experimental data derived from cathode erosion studies are highly contradictory because, along with the ion erosion, the cathode material is carried away in the form of macroparticles, droplets, and neutral vapor during discharge operation. The neutrals escaping from the cathode spot region have thermal velocities (of the order of 10^5 cm s^{-1}) and obey the Maxwellian velocity distribution [37, 38].

When studying the emission of neutrals, Eckhardt [39] arrived at the conclusion that, while the ion source is the spot itself, only the hot inactive surface — the trace of the spot — can be the source of neutrals. The neutral fraction in the total erosion is small: in several experiments it has been possible to estimate its upper bound, because it proved to be smaller than the measurement error. According to the data of Ref. [36], the emission of neutrals accounts for less than 1% of the total mass loss, and according to Ref. [40] for several percent as a maximum. Since the hot trace of a spot or a droplet is believed to be the source of neutral vapor, the neutral fraction in the erosion is an alternating quantity.

The term ‘macroparticles’ in the scientific literature is applied to solid particles and liquid metal droplets [4, 41]. The cause for solid particle production is the thermoelastic stress which exceeds the ultimate strength of the cathode material [41]. The fraction of these particles in the total cathode erosion is not large. A substantial part of the cathode material escapes from the cathode spot region in the form of liquid metal droplets [36, 37, 42–44]. The dimension of escaping droplets varies over a wide range: the lower limit is defined by the instrumental resolution [37], and the upper limit depends on the arc operating conditions. Specifically, the droplets with diameters of more than 100 μm emanate from a strongly heated cathode region [42].

The droplet fraction in the cathode erosion depends, like the neutral fraction, on the discharge current, the character of spot motion, the cathode melting temperature or, in other words, on the degree of heating of a local cathode region and the quantity of liquid metal in this region. Accordingly, the commonly used techniques of the erosion investigation, like weighing and evaluation from the variation of geometric parameters of erosion structures, largely depend on the arc current, the duration of discharge operation, and the cathode geometry.

2.3.3 Ion erosion. Daalder [45] conducted a series of experiments with copper cathodes 25 and 10 mm in diameter. The arc current was varied between 33 and 200 A. The mass loss M was measured by the weighing technique, and then this mass was divided by the electric charge flowed q to determine the specific mass loss. As a result, the dependence of the erosion rate γ on the electric charge flowed was derived (Fig. 3).

It turned out that the dependences obtained in different conditions yield the same value of the erosion rate $\gamma = 40$ μg C^{-1} as the electric charge flowed q is lowered to 0.1 C. Daalder [45] suggested that the lowest erosion values from amongst the large number of erosion rates measured by many authors with different materials give the ion erosion rate γ_i.

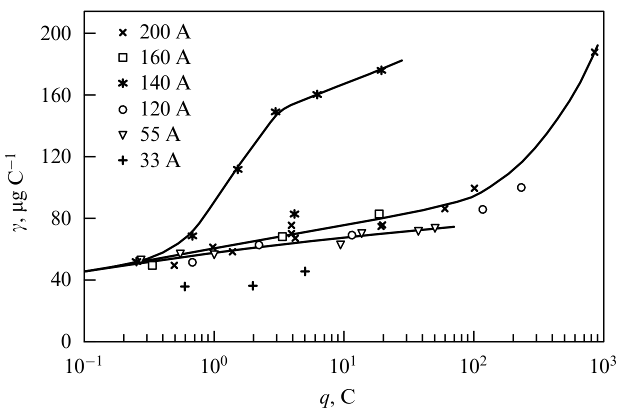

Figure 3. Erosion rate for a copper cathode as a function of the quantity of electricity flowed through an arc for the arc currents of 200, 160, 120, 55, and 33 A (the cathode was 25 mm in diameter), 33 and 140 A (the cathode was 10 mm in diameter) [45].

We note that the ion erosion rate is best determined at the lowest possible quantities of electricity flowed. The least-erosion data are collected in Table 4. The γ_i values in the first column were obtained from the minimal erosion measured by different authors, and in the second column from the measurements of Daalder [45].

Table 4. Minimal cathode erosion rate which is interpreted as the ion erosion rate [45].

Cathode material	γ_i, μg C^{-1} (minimal erosion)	γ_i, μg C^{-1} (borrowed from Ref. [45])
Cd	130	128
Zn	76	74.5
Al	25	22
Mg	25	19
Ag	108	90.4
Cu	35–40	39.2
Ni	50	48.9
Mo	47	55
Fe	50	40
W	62	90
C	16–17	13

The results of a detailed investigation into the erosion characteristics in the spark stage of a vacuum discharge are given in Ref. [22]. The experiments were performed with cylindrical tips, which enabled an easy determination of the mass loss from the decrease of the cylinder height.

The employment of a pulsating current mode with short-duration current pulses eliminated the cathode erosion in the form of liquid metal droplets and neutral vapor. This allowed a conclusion that the erosion rates thus measured represent the values of precisely the ion erosion rate. The measurement results turned out to be very close to the data given in Table 4. In particular, the γ_i value for a copper cathode was found to equal 40 μg C^{-1}.

The value of the ion erosion rate can be determined from the observed data on the ion current and average ion charge in arc plasma experiments with the aid of the obvious formula

$$\gamma_i = \frac{i_i}{i} \frac{m_i}{Ze} . \qquad (3)$$

A correction was made in Ref. [40] for the ion-to-arc current ratio. Since all the ions were extracted from the interelectrode space in the experiments of Refs [34, 35], the i_i/i ratio proved to be somewhat higher. However, this increase is insignificant and the i_i/i ratio can be taken to equal 0.1. In view of this correction, formula (3) assumes the form

$$\gamma_i \approx 0.1 \frac{m_i}{Ze} . \qquad (4)$$

Therefore, the ion erosion rate is only determined by the average ion charge Z and the ion mass m_i.

The above reasoning regarding the ion erosion applies to cathode spots of the second type. For spots of the first type, the erosion rate is substantially lower (of the order of 1 μg C^{-1}) and is below the data of Refs [40, 45], depending on the degree of contamination of the cathode surface.

3. Ectonic processes in vacuum arcs

3.1 Physics of cathodic processes

3.1.1 Cyclic processes in a cathode spot. Numerous experiments revealed that the properties of a vacuum arc, including the ion flow parameters referred to in the preceding section, are determined almost entirely by the processes in a small, brightly glowing region on the cathode whereby the current transfer between the cathode and the interelectrode gap is accomplished [1–4]. This region, which has come to be known as a cathode spot, comprises the active segment of the cathode surface, heated to temperatures far exceeding the melting temperature, as well as the near-cathode plasma resulting from the evaporation of the active segment. The cathode spots are in constant motion; however, this motion is apparent, in reality some spots die off while the others emerge.

It is the practice to recognize cathode spots of the first and second types [46]. Spots of the first type occur on the cathodes with dielectric films and inclusions. They leave behind many small craters spaced some distance apart, which are characterized by small values of the erosion rate (not exceeding 10^{-6} g C^{-1}). Spots of the second type emerge on well cleaned and degassified cathode surfaces. The values of the erosion rate for spots of this type are of the order of 10^{-4} g C^{-1}. The traces of the cathode damage (craters) either superimpose on one another, or touch one another.

The subject of our review is the spots of the second type, because discharge operation has the effect that the cathode is cleaned from dielectric inclusions, films, etc., leading to the disappearance of the spots of the first type. The characteristic time scale of the processes in cathode spots is of the order of 10^{-9} s, and the spatial scale of the order of 10^{-4} cm [3]. This imposes the corresponding requirements on the spatial and time resolution of the measuring equipment employed in the experiments. Considered below are primarily the experimental results satisfying these requirements.

A significant role for understanding the physics of a vacuum arc is played by the threshold current i_{th} and the cathode drop U_c. These quantities determine the lowest energy expenditure needed for the operation of an arc discharge. The threshold current i_{th} is the minimal current whereat the arc discharge will be self-sustained. The threshold current magnitude ranges between tenths of an ampere and several amperes, depending on the cathode material [1, 3].

The cathode drop U_c is the lowest voltage in the cathode region of the arc. The main feature of the cathode drops for different cathode materials is that they are close, to an order of magnitude, to the value of the metal ionization potential U_i. The ratio U_c/U_i for all metals falls within the range from 0.8 to 3. The length of the voltage drop region is estimated as 10^{-4} cm [1, 3].

During arcing there occurs a cyclic potential variation in the cathode region. For instance, for a copper cathode (Fig. 4) and near-threshold currents, the oscillations manifest themselves in the cyclic appearance of voltage peaks with an amplitude of 5–20 V against the background of a stable cathode drop $U_c = 16$ V [47]. The average cycle duration amounts to 30 ns [3, 47]. A consequence of the potential oscillations in the cathode region is the occurrence of a noise spectrum against the background of stable discharge operating voltage.

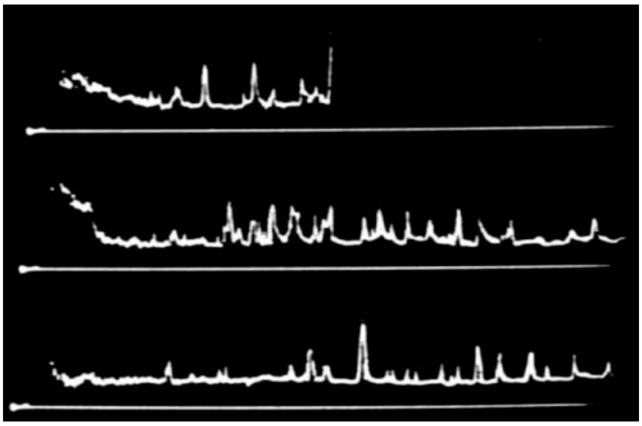

Figure 4. Typical oscillograms of the voltage drop across a vacuum arc with copper electrodes in the threshold current domain [47]. The arc current is 4 A.

An investigation of the amplitude noise spectra at frequencies up to 300 MHz revealed two specific features taking place for a copper cathode at 39.5 and 57 MHz [48]. This corresponds to oscillation periods of 25 and 17 ns and confirms the existence of two characteristic intervals in the oscillation cycle of the cathode potential. The occurrence of similar features in the amplitude noise spectrum was also established for a tungsten cathode for which the cycle duration equaled 25 ns, and the upward potential jumps amounted to 50 V [47].

The occurrence of pulse-like upward potential jumps and ensuing cyclicity of the processes in the cathode spot is a manifestation of an intrinsic discharge instability. The electric potential increase is an indication that the discharge experiences periodic crises, and a higher potential is required for a short period for its self-maintenance. The potential build-up in the near-cathode region is attended with a strengthening of the ion current to the cathode.

The decisive role of the ion current to the cathode (Fig. 5) in the initiation of new cathode spots was convincingly

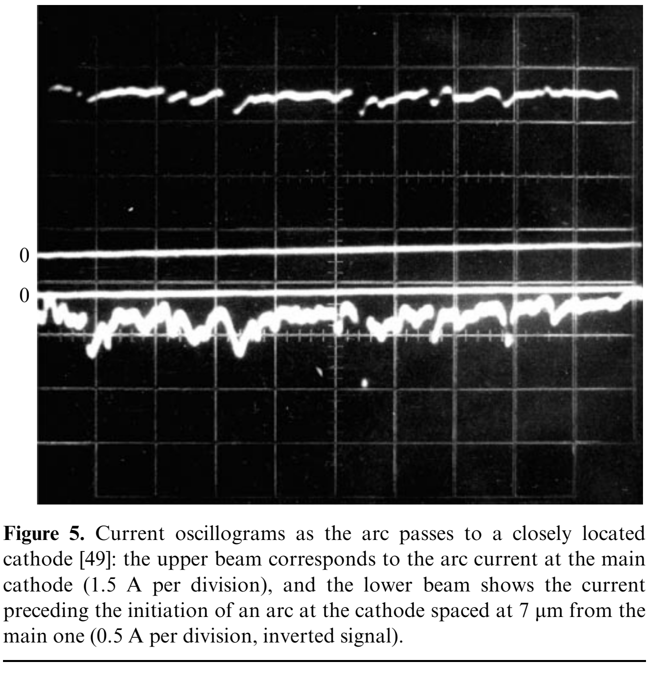

Figure 5. Current oscillograms as the arc passes to a closely located cathode [49]: the upper beam corresponds to the arc current at the main cathode (1.5 A per division), and the lower beam shows the current preceding the initiation of an arc at the cathode spaced at 7 μm from the main one (0.5 A per division, inverted signal).

demonstrated in Ref. [49] which investigated the transfer of an arc from one cathode to another spaced at $\lesssim 7$ μm. According to the authors' estimates made from the crater dimensions at the second cathode in the pre-arc stage, this transfer takes place when the ion current density exceeds 10^7 A cm^{-2}. It is evident that an ion current of this density provides the energy density at the cathode required for the initiation of new cathode spots. The most dramatic manifestation of intrinsic instability of the discharge is its spontaneous extinction.

3.1.2 Cathode spot structure. An important property of a cathode spot is the existence of an internal structure — separate cells or fragments of the cathode spot. The existence of the cathode spot substructure was discovered in the investigation of erosion structures which an arc left behind at thin-film cathodes [1]. According to I Kesaev, each cell of a cathode spot carries a current equal to the doubled threshold current of an arc operation, $2i_{\text{th}}$.

The availability of a spot substructure has long been in doubt. One of the arguments adduced in this case is the existence of the ultimate current, above which a new cathode spot is produced to operate simultaneously with the old one. Harris [2] made up a list of ultimate currents for different cathodes. For instance, the respective ultimate currents for Al, Cu, Fe, Mo, W, and Ag metals correspond to 50, 75 – 100, 60 – 100, 150, 300, and 60 – 100 A. At present there exist many facts that prove that high currents also involve the operation of a large number of cells in the cathode spot.

The existence of cells manifests itself in the occurrence of microcraters in the spot region. These microcraters were observed by many authors under a variety of arc operating conditions (a current of $1 - 10^3$ A, a duration of $10^{-8} - 10^{-2}$ s, different cathode materials, etc.) [1 – 4]. The availability of the ultimate current suggests that there is some mechanism that tries to hold together a large number of cathode spot cells [50]. The point is that the grouping of the cells in a cathode spot affords conditions energetically more advantageous to their reproduction. A thus collectivized cathode spot exhibits higher values of the average current density, the cathode surface temperature, and the near-cathode plasma concentration.

Jüttner [10, 51, 52] obtained a direct confirmation of the existence of cathode spot cells with lifetimes in the nanosecond range. He employed image-converter tubes and laser absorption techniques to study the structure of the cathode spot.

Figure 6 displays the dynamics of variation of the cathode spot structure for a vacuum arc with a copper cathode and an arc current of 30 A. Investigating the fluctuations of the light flux emitted by the cathode spot revealed that there emerge five light intensity peaks during a time period of 50 ns. The occurrence of the latter peaks is a consequence of the production and extinction of cathode spot cells.

3.1.3 Near-cathode plasma parameters. As noted above, the operation of cathode spot cells is accompanied by the emission of plasma jets, whose velocity of directed motion is of the order of 10^6 cm s^{-1}. In this case, the distribution of plasma parameters is extremely nonuniform. According to Vogel [53], the plasma number density in the immediate vicinity (at a distance of 1 μm) of a copper cathode is, by the order of magnitude, equal to 10^{22} cm^{-3}.

Taking advantage of laser diagnostics, Anders et al. [54] showed that the plasma number density at a distance of 5 μm from the copper cathode amounts to $(3-6) \times 10^{20}$ cm^{-3}. These results testify to the existence of a nonideal plasma in the region of cathode spot operation. The ion concentration falls off as r^{-2} with distance to the cathode.

Puchkarev [55] employed probe diagnostics to find out that the electron temperatures within 0.1 mm from the vacuum arc spot amount to 4.6 ± 0.5 and 5.8 ± 0.5 eV for copper and tungsten cathodes, respectively. Away from the cathode this temperature lowers to $1 - 2$ eV [4].

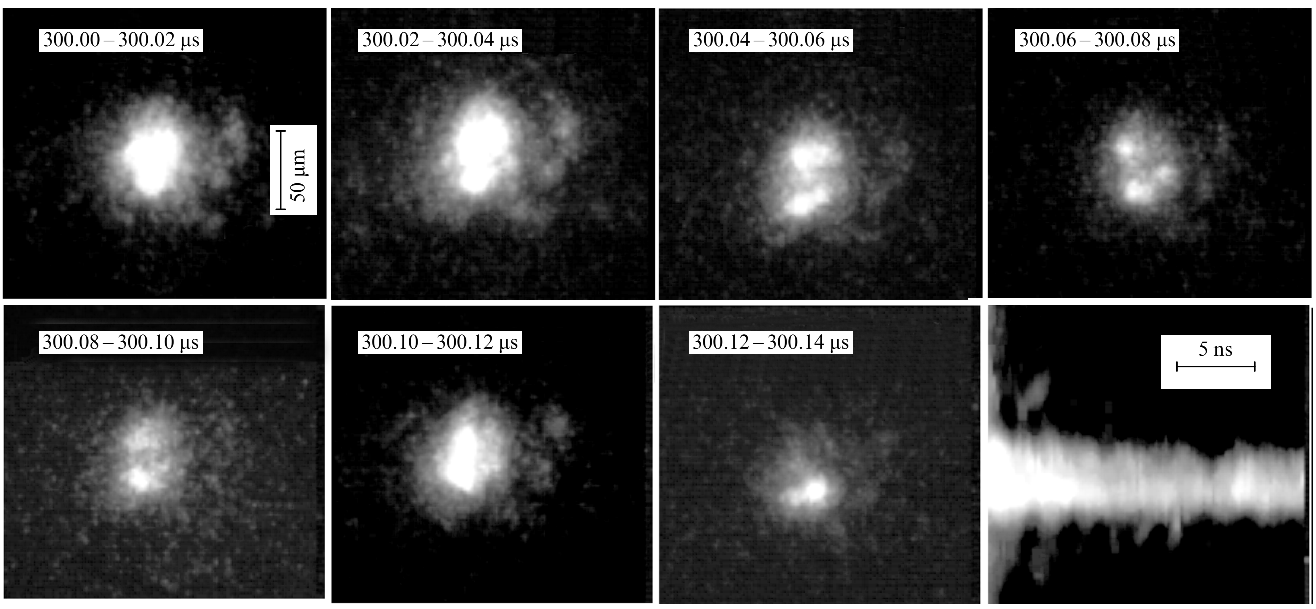

Figure 6. Dynamics of variation of the internal structure in a cathode spot at a copper cathode for a current of 30 A after 300 μs since the arc initiation. The time of exposure is 20 ns [10].

3.1.4 Liquid metal fraction of the cathode spot. The reactive force arising in the expansion of high-velocity plasma jets exerts pressure on the liquid metal produced due to the cathode heating in the region of spot cell operation. Under this pressure, the liquid metal splashes out in the form of droplets and jets from the cathode spot region.

The current build-up results in the enlargement of droplets, and therefore of interest are those papers in which the arc current was close to the threshold one. This applies primarily to the paper by Utsumi and English [37], in which experiments were conducted for a current of 2–6 A. A study was made on particle size and velocity distributions and also on the number of particles which is accounted for by a unit charge flowed for Au, Pd, and Mg cathodes. The highest observable velocities of droplet expansion were found to equal 4×10^4, 4.5×10^4, and 10^4 cm s^{-1}, respectively, while the most probable velocities amounted to 2.5×10^4, 3.5×10^4, and 0.5×10^4 cm s^{-1}. The number of droplets per unit charge flowed was $(1.5-2) \times 10^7$ C^{-1}.

McClure [56] estimated the pressure arising from the reactive force of the ion flow to arrive at a value of $p \approx 2 \times 10^8$ Pa, which corresponds to the droplet expansion velocities at a level of 10^4 cm s^{-1} found experimentally. Mesyats [57, 58] surmised that the droplets play a significant part in the self-maintenance of an arc discharge. The cycle duration in a cathode spot cell in this case was estimated at 20–30 ns, which is close to the measurement data obtained by different techniques.

3.1.5 Current density in a cathode spot. The governing characteristic of the mechanism of energy release in a cathode spot is the current density at the point of its lashing down. For current densities above 10^8 A cm^{-2}, the bulk ohmic heating prevails [3, 59]. A surface source operating due to the ion energy has to be invoked for lower current densities [4]. The difficulties encountered in measuring the current density stem from the fact that direct measurements of the current density are not feasible owing to the small size of separate fragments of the cathode spot as well as to its chaotic and fast motion over the cathode surface.

Experimental estimates of the current density in the cathode spot of a vacuum arc underwent changes over the years. Beginning in the 1920s with the progress in time and spatial resolution of experimental techniques, there was a tendency for the increase in experimentally determined current density: from 10^3 to 10^8 A cm^{-2} at the present time.

So wide a scatter in the measurement data is indicative, on the one hand, of the limitations of techniques employed to measure the current density and, on the other hand, of the uncertainty as to the very notion of the current density in a cathode spot. The point is that, owing to the existence of a substructure in a cathode spot, really meaningful, from a physical standpoint, is the current density in its separate cell.

The measurements of the current density are commonly performed for a single cathode spot, wherein the current is known, and therefore the goal of the measurements is to determine the emissive surface area. The latter is evaluated by measuring the glow region diameter or from the dimensions of craters which remain on the cathode surface. However, the current densities calculated using this data as the base are inaccurate: first, it is doubtful whether all microcraters in the cathode spot are produced simultaneously and, second, one can hardly say with certainty that the arc current is uniformly distributed over the entire glowing region and that the

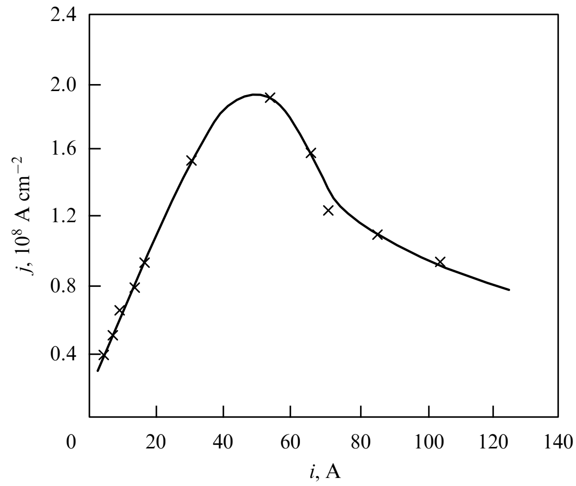

Figure 7. Current density as a function of the cathode spot current in a vacuum arc with a copper cathode [60].

glowing region exists throughout all the period of arc operation. The current density measurements, with the use of these techniques, merely yield the lower bound of the current density.

Despite the above remarks, the current density is quite often determined from the crater area. For instance, using the current–crater radius dependence, Daalder [60] calculated the dependence of the current density $j(i)$. According to this dependence, the current density is 0.4×10^8 A cm^{-2} for a near-threshold current, peaks at 2×10^8 A cm^{-2} for a current of 50 A, and falls off anew to 0.9×10^8 A cm^{-2} for a current of 100 A (Fig. 7).

Kesaev [1] measured the current density at a copper film cathode from the dimension of the imprint of a cathode spot with one cell to arrive at a value of $j \approx 10^7$ A cm^{-2}. He then solved the heat problem and showed that the actual current density was no less than 10^8 A cm^{-2}.

Strong evidence that the current density in the cathode spot of a vacuum arc in the final stage amounts to 10^7–10^8 A cm^{-2} is provided in the papers by Vogel and Jüttner [61], Sanger and Secker [62], Mesyats et al. [63], and also by many other authors (see, for instance, Ref. [4]). In particular, Mesyats et al. [63] staged a correct experiment to evaluate the current density in the arc, employing a pointed tungsten cathode. The experiments were conducted in vacuum at 10^{-8} Torr. The cathode was preheated to a temperature of 2000 K. The duration of arc operation did not exceed one or several cycles, while the current was varied between 0.5 and 5 A. The anode was a tungsten ball 0.3 mm in diameter produced by pulsed meltdown of a wire tip. A visual inspection of the pointed cathode revealed no traces of plasma action on the side surface. This signifies that the current flowed only through the summit of the tip. The current density was found to be $j \approx (2-10) \times 10^7$ A cm^{-2}.

3.1.6 Parameters of the cathode spot of a vacuum spark. In conclusion we list the parameter values of the cathode spot for a vacuum spark [22]: threshold currents – several amperes, the cathode voltage drop — tens of volts, the plasma expansion velocity of the order of 10^6 cm s^{-1}, the erosion rate reaching 10^{-4}–10^{-5} µg C^{-1}, the expansion velocity of liquid metal fraction of the order of 10^4 cm s^{-1}, the number of droplets per unit charge flowed of the order of 10^7 C^{-1}, the plasma number density in the spot region of the order of 10^{21} cm^{-3}, the microcrater radii of the order of 10^{-4} cm, the current density in the spot no less than 10^8 A cm^{-2}, and the cycle length about 10 ns.

A comparison of the parameters of the cathode processes in vacuum arcs and sparks allows a conclusion that in both cases we are dealing with the same phenomenon — explosive electron emission. The main source of energy release in the cathode spot is the ohmic heating caused by the high current density in the region of its operation.

3.2 Ectonic model of a cathode spot

3.2.1 Parameters of ectonic processes. Studying the phenomenon of explosive electron emission [3, 5–8, 22, 64] made it possible to substantiate the nature of physical processes in the cathode spot of a vacuum arc. The central tenets of the ectonic model, which is reliant on explosive emission processes, were formulated in Refs [3, 57, 58]. According to this model, the self-maintenance of a vacuum arc discharge takes place due to the explosion of liquid metal jets expelled from the region of cathode spot operation.

Explosive electron emission is initiated when a jet interacts with a near-cathode plasma. The jet surface closes the ion current from the plasma; in this case, there occurs an enhancement in current density at the base, depending on the geometrical jet shape. If the jet has the shape of a cone, the current density enhancement factor at the juncture is l/r, where l is the length of jet cone generatrix, and r is the radius at the juncture. In reality, the current density enhancement effect proves to be even stronger, because the jet gives rise to the current of thermal electron emission and, in addition, closes the current of backward electrons from the plasma.

However, the strongest effect on current density enhancement is supposedly exerted by the process of droplet separation from the jet. Schematic of the liquid metal jet with a droplet is given in Fig. 8. At the instant of droplet separation, the current density at the jet–droplet juncture increases by a factor of $4R^2/r^2$ in comparison with the current density received by the cathode (where R is the droplet radius, and r is the radius of the circle at the juncture section). Estimates show that the current density enhancement factor in the latter case may be as great as $\beta_j \approx 10^2$ and over. If this effect is accounted for, the density of current traversing the jet may range up to about 10^9 A cm^{-2}, resulting in the explosion of the liquid metal jet in a time of the order of 10^{-9} s and in the emergence of explosive electron emission.

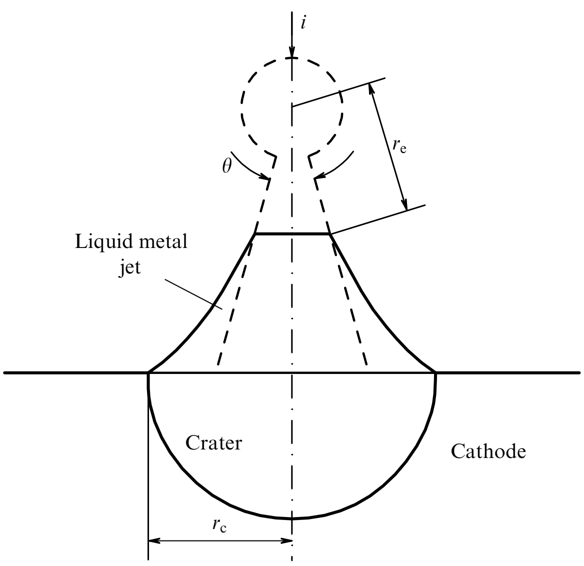

Figure 8. Model of a liquid metal jet whereupon the ecton operates: r_c is the melt radius at the cathode, and r_e is the radius of the ectonic region.

To qualitatively estimate the parameters of explosive electron emission, the energy expended in destroying the cathode material should be determined. This quantity is impossible to measure directly in the cathode spot region, but the information desired can be gained from the experimental data derived in studies of the exploding wires.

Despite different existence conditions, the same kind of energy release underlies the explosive electron emission (like the electric explosion of conductors) — the ohmic heating, which leads to the electric explosion of the metal. A specific action of current is required to convert a material from one energy state to another in the ohmic heating [65–67]:

$$\frac{\rho}{\varkappa}\,\mathrm{d}w = j^2\,\mathrm{d}t\,, \tag{5}$$

where w is the specific energy, ρ is the material density, $\varkappa$ is the resistivity, and j is the current density.

Under adiabatic heating, when the material characteristics depend only on the density w of the energy inputted, i.e. $\varkappa = \varkappa(w)$ and $\rho = \rho(w)$, the specific current action is expressed as follows

$$\bar{h} = \int_{w_0}^{w} \frac{\rho(w)}{\varkappa(w)}\,\mathrm{d}w = \int_0^t j^2\,\mathrm{d}t\,. \tag{6}$$

The quantity $\bar{h}$ in this case characterizes the physical properties of the given metal in the course of electric explosion.

Assuming that the values of material density ρ and heat capacity c are constant, and that the material resistivity is a linear function of the temperature, $\varkappa = \varkappa_0 T$, we are led to the simple relationship

$$\bar{h} = \frac{\rho c}{\varkappa_0}\ln\frac{T_{\mathrm{cr}}}{T_0}\,. \tag{7}$$

Here, T_{cr} is the critical temperature whereby there occurs the metal explosion, and T_0 is the initial temperature.

Invoking the analogy with the electric conductor explosion, the current density in the initiation of an ecton can be estimated from the formula for the specific action:

$$j = \left(\frac{\bar{h}}{t_{\mathrm{d}}}\right)^{1/2}, \tag{8}$$

where t_{d} is the explosion delay time. Since for the majority of metals the value of $\bar{h} \sim 10^9$ A^2 s cm^{-4} [67], for $t_{\mathrm{d}} \approx 10^{-9}$ s the current density is of the order of 10^9 A cm^{-2}.

The high current density results in the rapid heating of the cathode microvolume and its explosion attended by explosive electron emission. In the course of the explosion there occurs an increase in the emission region, the current density decreases, and the heat removal due to thermal conduction becomes significant, as does the energy removal due to the ejection of plasma and heated liquid metal. That is why the explosive emission current terminates to form a short-duration portion of electrons — an ecton.

The ecton lifetime can be estimated as follows [3, 57, 58]

$$t_{\mathrm{e}} = \frac{i_{\mathrm{e}}^2}{\pi^2 a^2 \bar{h} \theta^4} \,. \tag{9}$$

Here, a is the thermal diffusivity of the cathode material, and i_{e} is the ecton current. When writing down formula (9), it was assumed that the ecton operates due to the explosion of the liquid metal tip of conic geometry with a small cone angle θ (see Fig. 8).

The mass carried away from the cathode in a time t_{e} is defined by the relationship

$$M_{\mathrm{e}} = \frac{2}{3\pi^2} \frac{i_{\mathrm{e}}^3 \rho}{(a\bar{h})^{3/2} \theta^4} \,, \tag{10}$$

where ρ is the cathode material density. The total charge of the electrons in the ecton is given by

$$q_{\mathrm{e}} = \frac{i_{\mathrm{e}}^3}{\pi^2 a^2 \bar{h} \theta^4} \,. \tag{11}$$

Since the self-maintenance of an arc discharge takes place due to the explosion of liquid metal irregularities, in formulas (8)–(11) for the parameters a, ρ, and h advantage should be taken of their values in the liquid state.

A consequence of the finiteness of ecton lifetime is the cyclicity of processes in the cathode spot. The first stage of the cycle is the time period t_{e} during which the ecton operates. The second stage of a shorter length is the time period t_{i} during which the ion current from the near-cathode plasma initiates a new ecton. In Fig. 9, to the ecton stage of the cycle there corresponds the lower voltage level, and to the ion stage the voltage bursts. The lower voltage level relates to the cathode drop and is due to the voltage drop across the nonideal plasma in the cathode spot region [3].

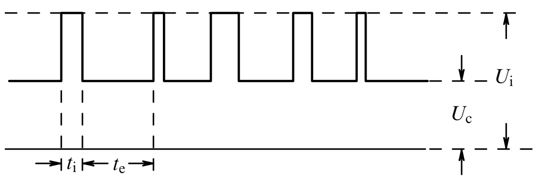

Figure 9. Schematic representation of the oscillation of the cathode potential in the cathode spot of a vacuum arc.

During the cycle when the voltage varies only slightly, the explosion of the liquid metal jet proceeds and the plasma flows out of the ecton operation region. A voltage burst signifies the termination of explosive electron emission. In this case, the electric current is provided by the electrons from the strongly heated region at the cathode and the arc plasma ions incident on the cathode surface. Furthermore, the ion current is responsible for the initiation of a new ecton due to the explosion of liquid metal irregularities in the spot region.

Based on the experimental data on voltage oscillations at near-threshold arc currents and on voltage noise, estimates were made regarding the cycle duration $t_{\mathrm{c}} \approx 30$ ns for copper and tungsten cathodes as well as the time fraction of the ion stage of the cycle: $\alpha = t_{\mathrm{i}}/(t_{\mathrm{i}} + t_{\mathrm{e}}) \approx 0.2$.

Another significant property of the cathode spot is the availability of an internal structure — the existence of separate cells, or fragments, of the cathode spot. According to Kesaev, every cathode spot cell carries a current equal to the doubled threshold current of arcing i_{th} [1]. In the context of the ectonic model, a spot cell is an explosive emission center which emits a portion of electrons — an ecton.

One of the principal arguments in support of the ectonic model is the availability of microcraters with a radius $r_{\mathrm{c}} \sim 10^{-4}$ cm in the imprint of a cathode spot. This is not only qualitative, but also quantitative testimony to the ectonic processes in the cathode spot. Indeed, if a microcrater is produced due to thermal conduction, the velocity of thermal boundary propagation would be 10^4 cm s^{-1}, and hence the production time of this crater would be $t_{\mathrm{c}} \sim 10^{-8}$ s. If the current through the cell is $i_{\mathrm{e}} = 2 i_{\mathrm{th}}$ and $i_{\mathrm{th}} \approx 1$ A [1], then the current density through the cell would be $j_{\mathrm{c}} \sim 10^8$ A cm^{-2}. These values of the parameters r_{c}, t_{c}, and j_{c} are the consequence of ectonic processes in the cathode spot of a vacuum arc.

3.2.2 Ion erosion and average ion charge. In the context of the ectonic model we can analyze the characteristics of the ion flux emitted by the cathode spot. The mass carried away from the cathode in a time t_{e} is defined by formula (10). For a time t_{i} there flows primarily the ion current to the cathode, which is approximately equal to 0.1 of the arc current, according to the data of Ref. [47]. Hence the total cathode mass loss during a cycle is $M_{\mathrm{e}}(1 - 2\alpha)$.

Therefore, in view of formulas (10) and (11) we can write the following expression for the specific ion erosion:

$$\gamma_{\mathrm{i}} = \frac{2}{3} \rho (1 - 2\alpha) \left(\frac{a}{\bar{h}} \right)^{1/2} . \tag{12}$$

Using formulas (3) and (12) it is possible to determine the average ion charge in the plasma produced due to the ecton operation:

$$Z = \frac{3}{2} \frac{i_{\mathrm{i}}}{i_{\mathrm{e}}} \frac{m}{e\rho(1 - 2\alpha)} \left(\frac{\bar{h}}{a} \right)^{1/2} . \tag{13}$$

Since the ratio $i_{\mathrm{i}}/i_{\mathrm{e}} \approx 0.1$ is true for practically all the cathode materials [34, 35], the values of γ_{i} and Z are independent of the current and are determined only by the characteristics of the cathode material, which is consistent with experimental data [23, 45].

Table 5 lists the average values of arc plasma charge and ion erosion obtained by formulas (12) and (13) for several metals, for which the magnitudes of specific action are known [3, 68]. The thermophysical metal coefficients were borrowed from reference book [69]. By analogy with W and Cu, the

Table 5. Ion erosion rate and average charge of an arc plasma for different cathode materials.

Cathode material	Cu	Au	Al	Ag	W
ρ, g cm^{-3}	8.0	17.2	2.3	9.3	17.0
a, cm^2 s^{-1}	0.42	0.40	0.40	0.56	0.14
$\bar{h}$, 10^9 A^2 s cm^{-4}	3.1	1.3	1.4	2.0	1.5
γ_{i}, μg C^{-1}	37.2	120.6	15.5	62.2	65.7
Z	1.76	1.69	1.80	1.77	2.90
Z [23, 24]	1.7–2.0	1.6–2.0	1.5–1.7	1.8–2.1	3.0–3.1

value of α was assumed to be 0.2 for all the materials. A good accord between the tabular data and the experimental results comes as a surprise if it is remembered that the values of thermophysical parameters of the materials involved were crudely determined from experiments.

3.2.3 Liquid metal – plasma interaction. The high density of explosive emission current implies a high energy density directly in the condensed phase. The fact that a fast energy input in metal can produce an energy density at a level of $w \sim 10^4$ J g^{-1} was confirmed by experiments on the exploding wires [67] and the explosion of microtips heated by the field emission current [22]. A theoretical analysis performed by Valuev and Norman [70] showed that the metal temperature in the condensed state prior to the onset of electric explosion can be as high as 1.7×10^4 K.

Mesyats [16] came up with a gasdynamic model of the cathode material expansion in the explosive electron emission, which states that the energy required for the initial plasma expansion is accumulated in the condensed phase. From the condition of total energy conservation in a volume occupied by particles it follows [71] that the velocity v of motion of the front layers is related to the specific energy through the formula

$$v = \left(\frac{4\mu}{\mu - 1} (w - w_s) \right)^{1/2} , \tag{14}$$

where w_s is the sublimation energy, and μ is the adiabatic index. According to formula (14), the velocity of front plasma layers (equal to 10^6 cm s^{-1}) is attained for $w \approx (2-3)w_s \sim 10^4$ J g^{-1}.

The reactive force of the plasma stream, referred to a unit current, is given by [3]

$$F = \frac{\gamma_i v}{2(1 - \alpha)} . \tag{15}$$

For copper material with $v \approx 10^6$ cm s^{-1}, the value of F is ≈ 23 dyn A^{-1}, which agrees well with the value of $F = 20$ dyn A^{-1} derived by Tanberg [11].

The pressure exerted by the force (15) on the surface of the liquid metal craterlet with a surface $S = \pi r_c^2 = 4\pi a(1 - \alpha) t_c$ can be estimated as follows

$$P_c = \frac{\gamma_i v i_e}{8\pi a (1 - \alpha)^2 t_c} . \tag{16}$$

For a copper cathode and an ecton current $i_e = 3.2$ A, the pressure will be $P_c \approx 10^8$ Pa, which agrees with the estimate made by McClure [56].

The pressure exerted on the cathode produces liquid metal jets and droplets due to metal sputtering. Their expansion velocity is defined by the relation

$$v_l = \left(\frac{2P_c}{\rho} \right)^{1/2} = \frac{1}{2} \left(\frac{\gamma_i v i_e}{\pi (1 - \alpha)^2 a t_c \rho} \right)^{1/2} . \tag{17}$$

For a copper cathode, one has $v_l \approx 1.5 \times 10^4$ cm s^{-1}, which is rather close to the experimental data on the expansion velocity of the droplet fraction [37].

Therefore, even during the ecton operation the conditions form for the regeneration of ectonic processes due to the interaction of liquid metal jets with the near-cathode plasma, which provides the self-maintenance of an arc discharge.

3.2.4 Ion velocities. Formula (14) gives an estimate of the velocity of motion of the plasma boundary layers due to the energy inputted in the condensed state. However, the bulk of the energy is inputted not in the condensed phase, but in the plasma state. The specific energy deposited in the cathode material in the region of cathode drop can be estimated as

$$w \approx \frac{i_e U_c t_e}{M_e} \approx \frac{U_c}{\gamma_i} \approx (1-5) \times 10^5 \text{ J g}^{-1} . \tag{18}$$

This energy is inputted primarily in the nonideal plasma state and goes into the heating and emission of electrons as well as the ionization and acceleration of ions [3].

During material expansion, its number density changes from the solid one to $10^{14} - 10^{15}$ cm^{-3}, which corresponds to the ideal plasma state. Because of a strong concentration gradient, the plasma expansion is close to the spherically symmetric one. Ion acceleration in a spherically symmetric plasma expansion was considered in Ref. [29].

The average ion velocity at a large distance r from the cathode is approximately given by the formula

$$v(r) \approx 3.5 \left[(5\Lambda i_e)^{2/5} \frac{Z^{7/5}}{m} \right]^{1/2} , \tag{19}$$

where the Coulomb logarithm $\Lambda \approx 5$ in the range of plasma parameters of interest, and the distance to the cathode is expressed in micrometers.

From formula (19) it follows that the ultimate velocity for a copper cathode ($i_e = 3.2$ A, $Z = 1.8$) is equal to 1.56×10^6 cm s^{-1}. The ion acceleration mechanism for a spherically symmetric expansion of the plasma emitted by micrometer-sized cathode spot cells was also considered in Ref. [72]. It was suggested that the electron temperature derived in the analysis of the charge-state ion distribution [26] may be used as one of the parameters, which is not quite justified in view of the strong nonuniformity of the plasma parameter distribution over the cathode spot region.

As shown above, the charge-state distribution and velocities of ion directed motion in arc plasmas produced in ectonic processes are formed primarily in the region of cathode voltage drop. According to different estimates, the length of this region does not exceed several micrometers. In the initial stage of expansion, a high energy density is accumulated in the plasma jet owing to the high number density of electrons and ions. This is responsible for an interesting phenomenon, which we refer to as the 'hunting effect'.

The effect consisting in the periodic emergence of glowing objects near the cathode was discovered by Batrakov et al. [74]. The investigation involving high-speed laser diagnostics revealed that these objects are dense plasma bunches with a plasma concentration close to 10^{20} cm^{-3}. An analysis of the interaction between liquid metal droplets and plasma jets in the near-cathode region of a vacuum arc, which was conducted in the context of the ectonic model, revealed that the heating of a droplet which finds itself in the region of the cathode spot operation can convert it to the plasma state [73].

Therefore, straightforward estimates of the ion parameters in vacuum arcs, made in the context of the ectonic model, agree well, both qualitatively and quantitatively, with experimental data. It must be emphasized that these estimates apply to a single cathode spot cell — an ecton. The arc current growth is accompanied by a simple increase in the number of simultaneously operating ectons, and therefore the ion parameters derived from experiments depend only slightly on the arc current up to a kiloampere current.

3.3 Simulation of ectonic processes

3.3.1 Erosion – emission model. The simplest model of an ecton operation due to ohmic heating cannot describe the diversity of physical effects in the cathode spots of vacuum arcs and sparks. The notion of near-cathode plasma parameters, cathode processes, and their evolution can be inferred only by way of numerical simulations. The difficulties encountered in the construction of a correct model of a cathode spot are evident, for its operation region harbors material in the condensed, liquid, gaseous, and plasma states. In this case, phase transitions proceed in micrometer-sized cathode segments within nanoseconds.

The first attempt to study cathode processes was the construction of erosion – emission model of an explosive emission center [75, 76]. The cathode heating by the flow of thermal-assisted field emission current was described by a system of equations covering thermal conduction, convective heat transfer by electron current, bulk heat release due to the Joule effect, and cathode material vaporization. The vaporization region and the emission region were assumed to coincide and be defined by the surface of a craterlet (pit) of the radius r_0. The boundary condition expressed the energy balance at the cathode surface, wherein account was taken of the energy fluxes carried by evaporable atoms, emission electrons, and ions traveling from the plasma to the surface.

In the case that the emissive capacity of the center exceeds the current carried away, this model implies the existence of a virtual cathode at the surface to repel the 'excessive' electrons, which is equivalent to augmenting the work function for the electrons. The electric field at the cathode was estimated by the well-known Mackeown formula. When solving the problem, the emission center was assumed to be somehow initiated, and therefore the current initially flowed through a hemisphere of radius 10^{-5} cm in the plane.

According to the calculations, the metal in the ecton region is strongly overheated early in the operation. This takes place due to intense ohmic energy release for a current density of the order of 10^9 A cm^{-2} and also due to the inertial behavior of vaporization. The surface disruption proceeds with a finite velocity (of the order of 10^5 cm s^{-1}) not exceeding the velocity of sound in the metal. That is why a significant amount of heat has time to be liberated in the superficial layer before this layer will be vaporized.

As the region of erosion and emission increases, the current density lowers, the heat release decreases, and the surface temperature also lowers, which is eventually responsible for the extinction of emissive capacity and the death of the center. It was assumed that the instant of death of the emission center came when the temperature and electric field at the cathode ceased to provide the requisite current. According to calculations, the duration of ecton operation lies primarily in the nanosecond range.

The temperature attained in the initial stage of ecton operation proved to be comparable with the binding energy of atoms (expressed in the appropriate units). According to the calculated results, a 10^{-5}-cm thick layer is heated from the initial temperature to several tens of thousands of kelvins and is vaporized in a time of the order of 0.1 ns. The metal density was assumed to remain invariable up to vaporization.

The high temperatures at the cathode surface early in the emission cycle, obtained in the calculations, were justly criticized, because they are more likely to demonstrate explosion-like behavior. Despite the incorrectness of applying the model to the overheating instability domain, it correlates well with experimental data on erosion rate and crater dimensions, which were measured from the melt boundaries for currents higher than 20 A. The agreement between calculations and experiments lent support to the conclusion about the decisive role of ohmic heating in these processes.

3.3.2 Hydrodynamic models of the initial stage of ectonic processes. The occurrence of high energy density in the cathode during explosive electron emission called for radically new transient hydrodynamic models with equations of state describing the thermodynamic material properties in the metal – plasma range.

The results of calculations for the initial stage of explosion of a pointed copper cathode in the context of a magnetohydrodynamic model were set out in Ref. [77]. Account was taken of the fact that the cathode material went through several stages of the phase state. Advantage was taken of a magnetohydrodynamic technique developed for exploding wires problems. The resistivity $\varkappa$ was assumed to be a function of the material density and specific thermal energy.

The shape of the function $\varkappa$ was determined using a calculative – experimental approach [67]. To take into account the two-dimensional character of material expansion, advantage was taken of a technique whereby two-dimensional effects were described by the combination of one-dimensional magnetohydrodynamic equations for the cylindrical case (the r-axis) and one-dimensional hydrodynamic equations for the plane case (the z-axis). The tip was divided into layers along the z-axis, which was aligned with the tip axis.

Calculations were performed for copper tips with a radius of the summit of 2×10^{-5} cm and the cone angles of 12°, 20°, and 40°. The time dependence of the current was assumed to be of the form $i = b + Kt$, where the parameter K was selected in such a way that the current density at the summit of the tip for $t = 0$ was 10^9 A cm^{-2}. For $K = 10^{10}$ A s^{-1}, by the time $t = 0.5$ ns there occurs an explosion of the tip summit and the production of a plasma with a specific energy of $(2-5) \times 10^4$ J g^{-1}. According to the calculated results, the temperature and average charge of the exploded material, which had a number density $n < 10^{21}$ cm^{-3}, lie in the ranges $T = 3-5$ eV and $Z \approx 2-3$, whilst the plasma expansion velocity is $(2-3) \times 10^6$ cm s^{-1}. Therefore, the magnetohydrodynamic calculation enables a correct estimate of the plasma parameters in the initial ecton formation stage.

It is significant that the specific action integral $\int_0^t i^2\,\mathrm{d}t$ by the time of explosion remains invariable under changes of the current. This is indication that the analogy to the electric explosion of a conductor, used in Section 3.3.1, is appropriate when analyzing ectonic processes. In the condensed state, the specific energy ranged up to a value of 8×10^3 J g^{-1}, which corresponds to a temperature of 1.8 eV for a specific heat capacity $c = 0.38$ J g^{-1} K^{-1}.

Paper [78] concerned with the simulation of aluminum-tip explosion constituted an extension of the technique outlined above. The mathematical description covering destruction of a microtip at the cathode in explosive electron emission involved the solution of a system of two-dimensional gasdynamic equations, which expressed the mass, momentum, and energy conservation laws in a differential form with the inclusion of electron and radiative heat transfer.

The thermal conductivity and electrical conductivity coefficients were calculated employing semiempirical formulas and tabular data [79–81]. To close the system of equations describing the dynamics of continuous media, advantage was taken of the wide-range equation of state of aluminum [81], which took into account the processes of melting, vaporization, and ionization. By and large, the calculations done coincided with the results of simulations outlined in Ref. [77].

In the most rigorous form, the problem of explosion-like expansion of the cathode material with the inclusion of continuous metal–plasma transition was solved in Refs [82, 83]. The calculations were performed for a copper cathode in the 3–7-A current range; the size and shape of initial microtips were chosen from the consideration that they should be the microirregularities produced in the operation of the previous ecton. The photographs of the cathode surface presented in Ref. [84] served as a basis for the selection.

To describe the electric explosion of the microirregularities, advantage was taken of the equations of two-dimensional nonstationary two-temperature magnetohydrodynamics and ionization kinetics [85]. The wide-range equation of the material state was constructed on the principle invoked in Ref. [86] and provided a good description of the material state ranging from the cold metal to hot plasma.

In general terms, the calculations yielded the following scenario of the electric explosion of a microirregularity at the cathode. Owing to a high current density, an intense ohmic heat release results in a rapid heating of the tip summit and a steep rise in pressure, which ranges into tens of gigapascals in a short period of time. A disruption wave travels towards the microtip base under the action of pressure. Expanding in the opposite direction is the plasma with the degree of ionization equal to unity, an initial electron temperature up to 10 eV, and a velocity of over 10^6 cm s^{-1}, which makes up a plasma flare.

Throughout the entire region of current flow from the cathode to the interelectrode gap there forms a layer of continuous metal–plasma phase transition, wherein the bulk of heat release takes place. The pressure in this layer is higher than the critical one, i.e. the material bypasses the domain of two-phase state and a sharp metal–plasma boundary is not formed. A smooth concentration variation and high temperatures have the effect that the metal–insulator transition has no time to be brought to completion prior to the onset of thermal ionization, and the degree of ionization remains relatively high. All this indicates that the ohmic nature of conduction is retained when the current flows between the metal and the plasma or, in other words, that there is no emission boundary between them.

With time the pressure in some metal–plasma transition domain lowers below the critical one, and inside it there begins the formation of an interface with an abrupt concentration front. A smooth ohmic transition has a lower resistance, and therefore the current across the metal–plasma junction begins to concentrate where this transition persists. And the notion of the ohmic nature of current flow in the emission center still holds.

The calculations yielded the following plasma characteristics in the cathode spot region. In the plasma phase, the electron and ion temperatures diverge significantly for concentrations lower than 3×10^{21} cm^{-3}. With time the electron temperature acquires a quasi-stationary profile with a peak equal to 5–6 eV at a distance of 1 μm from the cathode. Next follows a smooth decrease to 3–4 eV at a distance of 8 μm from the cathode. The ion temperature amounts to 3 eV in the region where the electron temperature reaches its maximum. The value of the specific ion erosion was found to be at a level of $(4-6) \times 10^{-5}$ g C^{-1}.

Figure 10 shows the spatial distribution of the average ion charge Z. The average ion charge amounts to 2.7–3 immediately after the explosion and lowers with time. The value of Z averaged over the cycle period is equal to 1.63. The calculated ion velocities range up to 2.1×10^6 cm s^{-1} at the initial point in time (Fig. 11).

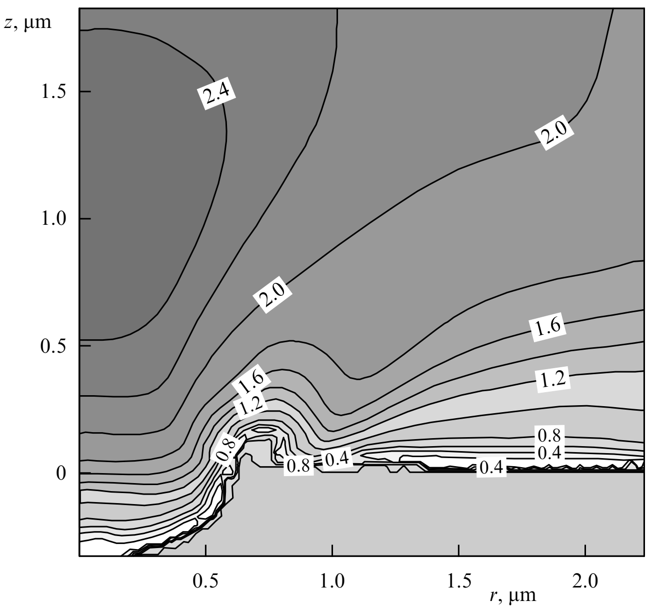

Figure 10. Distribution of the average ion charge early in the expansion of a cathode plasma [83].

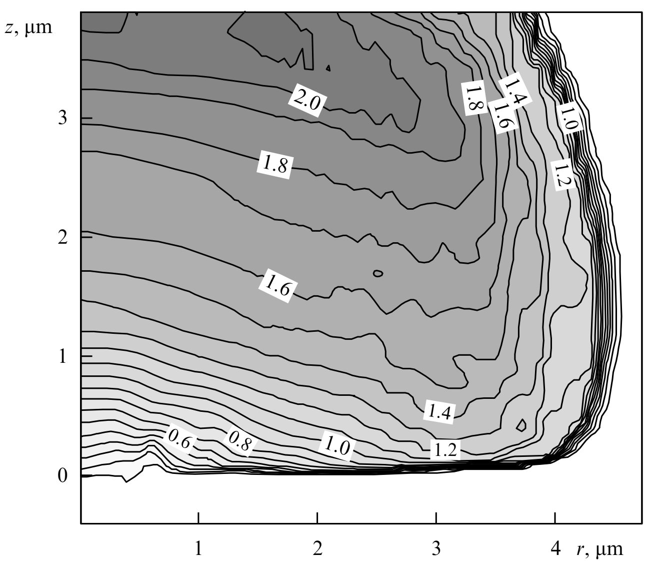

Figure 11. Distribution of ion velocities (in units of 10^6 cm s^{-1}) early in the expansion of a cathode plasma [83].

3.3.3 Hydrodynamic model of a cathode plasma jet. The results of simulation [82, 83] give the researcher an insight into the initial stage of plasma expansion. Because of the technical difficulties related to the strong nonuniformity of the plasma parameter distribution, the computational mesh was limited to a distance of 8 μm from the cathode. In this connection Barengol'ts et al. [29] performed numerical simulations of the processes in a plasma jet by solving a system of equations of two-dimensional, two-temperature hydrodynamics.

The averaged plasma parameters derived in the context of the model of Refs [82, 83] were employed as the boundary conditions. In the calculations, a subsonic ion flux and a given electric current were assumed to flow into the computation range through a cylindrical tube of radius $r_0 = 1$ μm and height $h = 0.5$ μm (the analogue of a crater). At the lower section of the tube (i.e. for $z = 0$), the flux has a given average charge $Z = 1$ and temperatures $T_e = T_i = 1.5$ eV, while the plasma number density is of the order of 10^{21} cm^{-3}.

The results of numerical simulation of the main parameters of an arc plasma are given in Fig. 12. We notice that they correlate rather well with the experimental data on ion parameters given in Refs [9, 23–25]. The average ion charge in plasma agrees with the data collected in Table 5. The ion velocity is somewhat higher than the value (1.28×10^6 cm s^{-1}) of Ref. [9]. However, in view of the wide scatter of experimental data, depending on the measurement technique and the vacuum conditions, the agreement with experiment is satisfactory.

We note that the plasma potential and temperature also correspond to experimental data [3, 4]. According to the calculations, the electron pressure gradient has the effect that the ions acquire velocities of directed motion of about 10^6 cm s^{-1} even at the distances of several micrometers.

Referring to Fig. 12, the average ion charge increases monotonically, the main ionization processes being confined to a distance of only 2 μm. Beyond 5 μm, the reactions terminate and there sets in the so-called 'quenching' of the ionic composition, which does not vary with further expansion. This is due to the fact that the reaction rates are proportional to the concentration (ionization) and to the concentration squared (recombination). As the plasma expands, its concentration falls off rapidly (as r^{-3} in the early stage). The reaction rates therefore decrease also, the recombination being suppressed more rapidly.

On acquiring a high charge at the jet base (where ionization state can be assumed to be in equilibrium), ions with a high velocity enter the region of slow reactions. But the time required for equilibrating the charge in this specific region is longer than the ion transit time. Therefore, the average charge in the plasma jet diverges significantly from the equilibrium one, depends on the velocity pickup rate, and cannot unambiguously reflect the plasma parameters in the cathode spot region, as was assumed in Ref. [26].

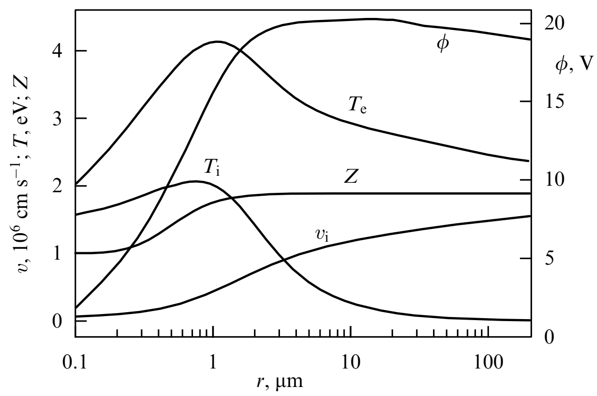

Figure 12. Arc plasma parameter distribution along the jet axis in the context of the hydrodynamic model [29].

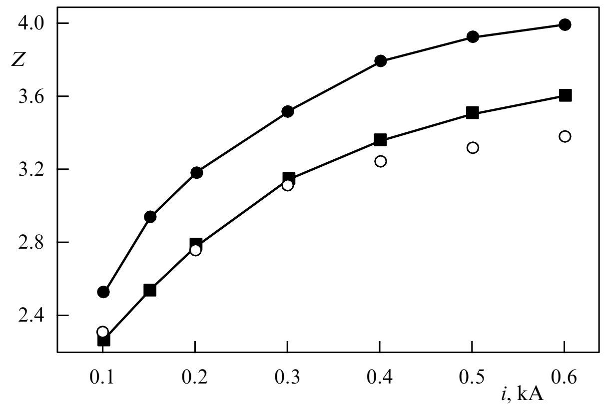

Figure 13. Average (squares) and peak (full circles) charges in an arc plasma embedded in an axial magnetic field [87]. The cathode is made of titanium, the magnetic field strength is 10 kG, and the empty circles represent the experimental data of Ref. [32].

Dedicated calculations performed to reveal the effect of an axial magnetic field showed that the fields under 10 kG have only an insignificant effect on the average charge in an individual plasma jet (the jet length is 100 μm, the current does not exceed 10 A, and the spot radius is 1 μm). In this connection, the hydrodynamic model was generalized to the case when the cathode spots are evenly distributed over the cathode surface [87].

Unlike a low-current arc (where ion parameters are determined by the processes in a single spot cell), the imposition of an external magnetic field has the effect that the 'freezing' of charge-state distribution does not set in and the average charge increases monotonically along the whole length of the collectivized plasma jet. In this case, the peak electron temperature exceeds 10 eV and is attained approximately half way along the interelectrode gap. The simulation results agree well with experimental data (Fig. 13).

4. Conclusions

Based on an analysis of ectonic processes, in this review we proposed a model of ion flow production in vacuum arcs. The ionic composition and the velocities of ion directed motion were shown to form due to explosion-like destruction of cathode microsegments in response to ohmic heating by high current density. In the operation of an ecton, in a short time (of the order of 1 ns) the cathode material sequentially passes through the condensed state as well as the nonideal and ideal plasma states.

Due to the energy stored in the condensed state (of the order of 10^4 J g^{-1}), the front layers of expanding plasma acquire a velocity of directed motion close to 10^6 cm s^{-1}. At the base of the plasma jet, the current density is rather high, and the cathode material continues to heat after the transition to the plasma state. The Joule energy released at this stage is the kinetic electron energy gained in the electric field. A part of this energy goes to ionize and heat the ions.

Ionization proceeds in a narrow, approximately micrometer-thick region near the cathode, and subsequently the ionic plasma composition undergoes no changes. The main contribution to the ion acceleration in the cathode plasma expansion is made by electron pressure gradient. Increasing the arc current up to a kiloampere is attended by a simple increase in the number of simultaneously operating ectons, which accounts for experimental data on the weak dependence of the ion flow parameters on the vacuum arc current.

Increasing the arc current above a kiloampere results in the contraction of a collectivized plasma jet due to the intrinsic magnetic field. Charge-state composition 'freezing' near the cathode does not take place in this case, and the average charge increases monotonically along the entire length of the plasma jet.

The authors are grateful to D L Shmelev and A M Murzakaev for their aid in preparing this review.

This work was partly supported by the Russian Foundation for Basic Research (grants Nos 02-02-17002 and 02-02-17509).

References

1. Kesaev I G *Katodnye Protsessy Elektricheskoĭ Dugi* (Cathode Processes in an Electric Arc) (Moscow: Nauka, 1968)
2. Lafferty J M (Ed.) *Vacuum Arcs: Theory and Application* (New York: Wiley, 1980)
3. Mesyats G A *Ektony v Vakuumnom Razryade: Proboĭ, Iskra, Duga* (Ectons in a Vacuum Discharge: Breakdown, Spark, and Arc) (Moscow: Nauka, 2000) [Translated into English: *Cathode Phenomena in a Vacuum Discharge: the Breakdown, the Spark and the Arc* (Moscow: Nauka Publ., 2000)]
4. Boxman R L, Sanders D M, Martin P J (Eds) *Handbook of Vacuum Arc Science and Technology: Fundamentals and Applications* (Park Ridge, N.J.: Noyes Publ., 1995)
5. Mesyats G A, Thesis for Doctorate of Technical Sciences (Tomsk: Tomsk Polytechnical Institute, 1966)
6. Bugaev S P et al. *Usp. Fiz. Nauk* **115** 101 (1975) [*Sov. Phys. Usp.* **18** 48 (1975)]
7. Litvinov E A, Mesyats G A, Proskurovskiĭ D I *Usp. Fiz. Nauk* **139** 265 (1983) [*Sov. Phys. Usp.* **26** 138 (1983)]
8. Mesyats G A *Usp. Fiz. Nauk* **165** 601 (1995) [*Phys. Usp.* **38** 567 (1995)]
9. Yushkov G Yu et al. *J. Appl. Phys.* **88** 5618 (2000)
10. Jüttner B *J. Phys. D: Appl. Phys.* **34** R103 (2001)
11. Tanberg R *Phys. Rev.* **35** 1080 (1930)
12. Kobel E *Phys. Rev.* **36** 1636 (1930)
13. Plyutto A A, Ryzhkov V N, Kapin A T *Zh. Eksp. Teor. Fiz.* **47** 494 (1964) [*Sov. Phys. JETP* **20** 328 (1965)]
14. Kassirov G M, Mesyats G A *Zh. Tekh. Fiz.* **34** 1476 (1964) [*Sov. Phys. Tech. Phys.* **9** 1141 (1965)]
15. Bugaev S P et al. *Zh. Tekh. Fiz.* **37** 2206 (1967) [*Sov. Phys. Tech. Phys.* **12** 1358 (1968)]
16. Mesyats G A, in *Proc. of the 10th Intern. Conf. on Phenomena in Ionized Gases, Oxford, England, Sept. 13–18, 1971* (Oxford: Henley-on-Thames, 1971) p. 333
17. Davis W D, Miller H C *J. Appl. Phys.* **40** 2212 (1969)
18. Kutzner J, Miller H C *J. Phys. D: Appl. Phys.* **25** 686 (1992)
19. Tsuruta K, Sekiya K, Watanabe G *IEEE Trans. Plasma Sci.* **PS-25** 603 (1997)
20. Bugaev A S et al. *Zh. Tekh. Fiz.* **70** (9) 37 (2000) [*Tech. Phys.* **45** 1135 (2000)]
21. Yang L, Zou J, Cheng Zh *IEEE Trans. Plasma Sci.* **PS-27** 882 (1999)
22. Mesyats G A, Proskurovsky D I *Pulsed Electrical Discharge in Vacuum* (Berlin: Springer-Verlag, 1989)
23. Brown I G *Rev. Sci. Instrum.* **65** 3061 (1994)
24. Brown I G, Galvin J E *IEEE Trans. Plasma Sci.* **PS-17** 679 (1989)
25. Brown I G, Godechot X *IEEE Trans. Plasma Sci.* **PS-19** 713 (1991)
26. Anders A *Phys. Rev. E* **55** 969 (1997)
27. Anders S, Anders A *J. Phys. D: Appl. Phys.* **21** 213 (1988)
28. Anders A *IEEE Trans. Plasma Sci.* **PS-29** 393 (2001)
29. Barengol'ts S A, Mesyats G A, Shmelev D L *Zh. Eksp. Teor. Fiz.* **120** 1227 (2001) [*JETP* **93** 1065 (2001)]
30. Nikolaev A G, Oks E M, Yushkov G Yu *Zh. Tekh. Fiz.* **68** (9) 24 (1998) [*Tech. Phys.* **43** 1031 (1998)]
31. Oks E M et al. *Appl. Phys. Lett.* **67** 200 (1995)
32. Oks E M et al. *IEEE Trans. Plasma Sci.* **PS-24** 1174 (1996)
33. Nikolaev A G, Oks E M, Yushkov G Yu *Zh. Tekh. Fiz.* **68** (5) 39 (1998) [*Tech. Phys.* **43** 514 (1998)]
34. Kimblin C W *Proc. IEEE* **59** 546 (1971)
35. Kimblin C W *J. Appl. Phys.* **44** 3074 (1973)
36. Tuma D T, Chen C L, Davies D K *J. Appl. Phys.* **49** 3821 (1978)
37. Utsumi T, English J H *J. Appl. Phys.* **46** 126 (1975)
38. Eckhardt G *J. Appl. Phys.* **44** 1146 (1973)
39. Eckhardt G *J. Appl. Phys.* **46** 3282 (1975)
40. Daalder J E *J. Phys. D: Appl. Phys.* **9** 2379 (1976)
41. Rakhovskiĭ V I *Fizicheskie Osnovy Kommutatsii Elektricheskogo Toka v Vakuume* (Physical Foundations of Electric Current Switching in Vacuum) (Moscow: Nauka, 1970)
42. Udris Ya Ya *Radiotekh. Elektron.* **6** 1057 (1963)
43. Klyarfel'd B N, Neretina N A, Druzhinina N N *Zh. Tekh. Fiz.* **39** 1061 (1969)
44. Golubchin G N, Sena L A *Elektrichestvo* (6) 60 (1956)
45. Daalder J E *J. Phys. D: Appl. Phys.* **8** 1647 (1975)
46. Lyubimov G A, Rakhovskiĭ V I *Usp. Fiz. Nauk* **125** 665 (1978) [*Sov. Phys. Usp.* **21** 830 (1978)]
47. Puchkarev V F, Proskurovskiĭ D I, Murzakaev A M *Zh. Tekh. Fiz.* **57** 1224 (1987); **58** 88 (1988) [*Sov. Phys. Tech. Phys.* **32** 736 (1987); **33** 51 (1988)]
48. Bochkarev M B, in *Proc. of the 17th Intern. Symp. on Discharges and Electrical Insulation in Vacuum, Berkeley, 1996* Vol. 1 (Piscataway, N.J.: IEEE, 1996) p. 151
49. Puchkarev V F, Bochkarev M B *J. Phys. D: Appl. Phys.* **27** 1214 (1994)
50. Mesyats G A, Barengol'ts S A *Dokl. Ross. Akad. Nauk* **375** 462 (2000) [*Dokl. Phys.* **45** 640 (2000)]
51. Jüttner B *J. Phys. D: Appl. Phys.* **28** 516 (1995)
52. Jüttner B *J. Phys. IV Colloq.* (Paris) **7** C4-31 (1997)
53. Vogel N *J. Phys. D: Appl. Phys.* **23** 1655 (1993)
54. Anders A et al. *IEEE Trans. Plasma Sci.* **PS-20** 466 (1992)
55. Puchkarev V F *J. Phys. D: Appl. Phys.* **24** 685 (1991)
56. McClure G W *J. Appl. Phys.* **45** 2078 (1974)
57. Mesyats G A *Pis'ma Zh. Eksp. Teor. Fiz.* **60** 514 (1994) [*JETP Lett.* **60** 527 (1994)]
58. Mesyats G A *IEEE Trans. Plasma Sci.* **PS-23** 879 (1995)
59. Litvinov E A et al. *Zh. Tekh. Fiz.* **48** 541 (1978)
60. Daalder J E *IEEE Trans. Power Ap. Syst.* **PAS-93** 1747 (1974)
61. Vogel N, Jüttner B *J. Phys. D: Appl. Phys.* **24** 922 (1991)
62. Sanger C C, Secker P E *J. Phys. D: Appl. Phys.* **4** 1940 (1971)
63. Mesyats G A et al. *Pis'ma Zh. Tekh. Fiz.* **11** 398 (1985)
64. Mesyats G A *Explosive Electron Emission* (Ekaterinburg: URO-Press, 1998)
65. Chace W G, Moore H K (Eds) *Exploding Wires* Vol. 1 (New York: Plenum Press, 1959)
66. Chace W G, Moore H K (Eds) *Exploding Wires* Vol. 2 (New York: Plenum Press, 1962)
67. Burtsev V A, Kalinin N V, Luchinskiĭ A V *Elektricheskiĭ Vzryv Provodnikov i Ego Primenenie v Elektrofizicheskikh Ustanovkakh* (Electrical Wire Explosion and Its Application in Electrophysical Facilities) (Moscow: Energoatomizdat, 1990)
68. Sedoi V S et al. *IEEE Trans. Plasma Sci.* **PS-27** 845 (1999)
69. Zinov'ev V E *Teplofizicheskie Svoĭstva Metallov pri Vysokikh Temperaturakh* (Thermophysical Metal Properties at High Temperatures) Reference Book (Moscow: Metallurgiya, 1989)
70. Valuev A A, Norman G É *Zh. Eksp. Teor. Fiz.* **116** 2176 (1999) [*JETP* **89** 1180 (1999)]
71. Zel'dovich Ya B, Raĭzer Yu P *Fizika Udarnykh Voln i Vysokotemperaturnykh Gidrodinamicheskikh Yavleniĭ* 2nd ed. (Physics of Shock Waves and High-Temperature Hydrodynamic Phenomena) (Moscow: Nauka, 1966) [Translated into English (New York: Academic Press, 1966)]
72. Krinberg I A *Zh. Tekh. Fiz.* **71** (11) 25 (2001) [*Tech. Phys.* **46** 1371 (2001)]

73. Mesyats G A, Barengol'ts S A *Pis'ma Zh. Eksp. Teor. Fiz.* **75** 306 (2002) [*JETP Lett.* **75** 257 (2002)]
74. Batrakov A V et al. *Pis'ma Zh. Eksp. Teor. Fiz.* **75** 84 (2002) [*JETP Lett.* **75** 76 (2002)]
75. Litvinov E A, Mesyats G A, Parfenov A G *Dokl. Akad. Nauk SSSR* **269** 343 (1983)
76. Litvinov E A, Mesyats G A, Parfenov A G *Dokl. Akad. Nauk SSSR* **279** 864 (1984)
77. Loskutov V V, Luchinskiĭ A V, Mesyats G A *Dokl. Akad. Nauk SSSR* **271** 1120 (1983)
78. Bushman A V et al. *Dokl. Akad. Nauk SSSR* **312** 1368 (1990)
79. Basko M M, Preprint ITÉF No. 145 (Moscow: Institute of Theoretical and Experimental Physics, 1985)
80. Bespalov I M, Polishchuk A Ya, Preprint IVTAN No. 1-257 (Moscow: Institute for High Temperatures, USSR Academy of Sciences, 1988)
81. Bushman A V et al. *Teplofizika i Dinamika Kondensirovannykh Sred pri Intensivnykh Impul'snykh Vozdeĭstviyakh* (Thermal Physics and Dynamics of Condensed Media under Intense Pulsed Actions) (Chernogolovka: Institute of Chemical Physics, USSR Academy of Sciences, 1983)
82. Shmelev D L, Litvinov E A *IEEE Trans. Plasma Sci.* **PS-25** 533 (1997)
83. Shmelev D L, Litvinov E A *IEEE Trans. Dielect. El. In.* **DEI-6** 441 (1999)
84. Puchkarev V F, Murzakayev A M *J. Phys. D: Appl. Phys.* **23** 26 (1990)
85. Silin V P *Vvedenie v Kineticheskuyu Teoriyu Gazov* (Introduction to the Kinetic Theory of Gases) (Moscow: Nauka, 1971)
86. Kolgatin S N, Khachatur'yants A V *Teplofiz. Vys. Temp.* **20** 447 (1982)
87. Shmelev D L, in *Proc. of the 19th Intern. Symp. on Discharges and Electrical Insulation in Vacuum, Xi'an, China, Sept. 18–22, 2000*, p. 218